EXPERIMENTAL INVESTIGATIONS OF NEUTRINO OSCILLATIONS AT A FISSION REACTOR

Thesis by

Heemin Kwon

In Partial Fulfillment of the Requirements

For the Degree of

Doctor of Philosophy

California Institute of Technology

Pasadena, California

1981

(Submitted Oct. 7, 1980)

ACKNOWLEDGEMENTS

The "ghost particles of the universe" could have never be detected by a single person. The work described in this thesis was carried out at the Institut Laue Langevin at Grenoble, France, in close collaboration with physicists from Caltech, Institut Laue Langevin, Institut des Sciences Nucléaires de Grenoble and Technische Universität München.

First of all, I would like to thank Professor Felix Boehm for providing me with this interesting thesis subject and supporting me throughout the experiment. I am grateful for his tremendous help in every respect.

The experiment would have not been possible without the enthusiasm and active support of Professor Rudolf Mössbauer.

Let me express my deep gratitude to Dr.Franz von Feilitzsch, Dr. Alan Hahn, and Dr. Jean-Luc Vuilleumier with whom I shared an office. I was influenced by their so distinct but complementary characteristics.

Important contributions and inspiring discussions with Dr. Jean-François Cavaignac, Dr. Dy-Holm Koang, and Dr. Bernard Vignon are greatly acknowledged.

I am indebted to Mr. Herbert Henrikson for his engineering works. I wish to thank Messieurs Christian Barnoux and Bernard Guerre-Chaley

for their technical and electronic assistance. I am also indebted to Mr. Ed Redden for his technical assistance in the early phase of the experiment. I am grateful to Mrs. Elsa Garcia's continuous help and logistical skill.

I would like to thank Dr. Petr Vogel for enlightening discussions.

The hospitality and generous support by many members of the Institut Laue Langevin has been immensely beneficial. I specially thank Madame Christel Kazimierczak for typing the thesis.

Financial support from the US Department of Energy and from the Alfred Sloan Foundation are appreciated.

Finally, I would like to thank my wife Sue-Ja for her endurance and encouragement.

ABSTRACT

To investigate the possibility of neutrino oscillations, the positron kinetic energy spectrum was measured using the inverse beta decay of the neutron ($\bar{\nu}_e + p \longrightarrow e^+ + n$) as a detector reaction. The experiment was carried out at the fission reactor of the Institut Laue Langevin at Grenoble, France. The well shielded detector was set up at 8.76 meters from the point-like reactor core in an antineutrino flux of 9.8×10^{11} cm^{-2} sec^{-1}. The target protons were provided by a liquid scintillator (total volume of 377 liters) which also served as a positron detector. The product neutrons were moderated in the scintillator and detected by ^3He wire counters via the $^3He(n,p)^3H$ reaction. A delayed coincidence was required between the prompt positron and the delayed neutron events. The positron energy resolution was 18% FWHM at 1 MeV. The signal to background ratio was better than one to one between 2 MeV and 6 MeV positron energy. With a counting rate of 1.56 counts per hour, 2919 $\pm$ 131 neutrino induced events were detected. The shape of the measured positron spectrum was analyzed in terms of parameters for neutrino oscillations. The experimental data are consistent with no oscillations. An upper limit of 0.2 eV^2 (90% c.l.) for the mass-squared differences of the neutrinos was achieved, assuming maximum mixing of two neutrino states. The ratio of the measured to the expected integral yield of positrons was determined to be $\int Y_{exp} / \int Y_{th} = 0.89 \pm 0.04$ (statistical) $\pm$ 0.13 (systematic).

To my father Taik Sang Kwon,

to my mother Chung Sook Kwon

and to all my family members.

TABLE OF CONTENTS

This thesis is divided into 5 sections. Chapter 1 gives a historical review of neutrino oscillations. Chapter 2 discusses a model of neutrino oscillations. Chapter 3 is devoted to a detailed description of the experiment. Chapter 4 presents the experimental positron spectrum, and compares it with the theoretical expectations. Results of he experiment are discussed in terms of parameters for neutrino oscillations. Future prospects are summarized in chapter 5.

CHAPTER 1

INTRODUCTION

Neutrinos have played an important role in understanding the theory of weak interactions. However, we are still challenged by fundamental questions about their properties. For example, do neutrinos have masses, and how many different neutrino types exist ? We now believe that there are at least three types of neutrinos, ν_e, ν_μ, ν_τ, with their corresponding antiparticles. They are produced by the weak interaction process in association with the electron, muon, and tau lepton, respectively.

One of the most fascinating questions today has to do with the possibility of oscillations between neutrinos (see Post Appendix). The idea of neutrino mixing was first considered by Nakagawa et al., and others[1], following the discovery of the existence of two kinds of neutrinos, ν_e, ν_μ[2]. Some years later, neutrino oscillations were independently proposed by Gribov and Pontecorvo[3] to explain the low flux of solar neutrinos[4]. The idea was that physical neutrinos are not pure states in a quantum mechanical sense, but superpositions of mass eigenstates. Accordingly, the physical neutrinos will oscillate in and out of their initial states, provided the mass differences of the pure states and the mixing amplitude between them are nonvanishing. But it is still not clear whether the solar neutrino puzzle is due to neutrino oscillations or to some other unknown mechanisms. Extended reviews on neutrino oscillations up to 1978 are contained in the paper by Fritzsch[5] and by Bilenky and Pontecorvo[6].

Only recently have neutrino oscillations been discussed extensively[7] (while this experiment was in progress) as being expected on theoretical grounds lending fresh momentum to the search for oscillations.

After the success of the SU(2) X U(1) Weinberg-Salam model[8] of the electroweak interaction, several more general models, attempting to unify the strong and electroweak interaction, have been proposed. According to some of these models (based on gauge symmetries), neutrinos are massive and could oscillate. Oscillations of the type $\nu_e \rightarrow \nu_\mu$ or $\nu_e \rightarrow \nu_\tau$ (flavor oscillations), or $\nu_e \rightarrow \bar{\nu}_{eL}$ (particle-antiparticle oscillations), or $\nu_e \rightarrow \bar{\nu}_{\mu L}$ (mixed oscillations) might be expected. (The symbol $\bar{\nu}_{eL}$ designates a wrong handed electron antineutrino.)

The present experimental limit on the masses of ν_e, ν_μ and ν_τ are 35 eV[9], 570 keV[10] and 250 MeV[11], respectively, which leaves ample room for the magnitude of various parameters describing neutrino oscillations. A recent experiment by Lyubimov et al.[12] suggests a finite mass of the electron neutrino in the range between 14 eV and 46 eV. However, this result is preliminary, awaiting confirmation.

Neutrinos also play an important role in the description of the early stage of the universe. Cosmological theories set limits on the neutrino masses[13] and the number of neutrino types[14]. The commonly accepted cosmological limit on the sum of the masses of neutrinos is 40 eV[15]. But the cosmological arguments should only be used as a guide.

The neutrino oscillation is also connected with the fundamental question of lepton number conservation because it violates the conven-

tional lepton number assignment. The mechanisms of $\mu \to e\gamma$ and the double beta decay are closely related to neutrino oscillations. Consequently, in some models (which do not have neutral heavy leptons), a limit on neutrino oscillations can impose more stringent limits on $\mu \to e\gamma$ and the double beta decay than the current experiments are able to provide.

From several recent experiments with high energy neutrinos, limits for the possibility of oscillations have been set. (These limits are sketched in Fig. 1. The variables used in this figure will be discussed below.) However, these limits are not sufficiently restrictive. It is the purpose of this experiment to provide an answer, with a better sensitivity, to the question: Is there evidence for oscillations of electron antineutrinos produced in a fission reactor ?

Recently, Reines et al.[16] claimed to have found evidence for $\bar{\nu}_e$ oscillations. Clearly, an independent confirmation of this observation is most important.

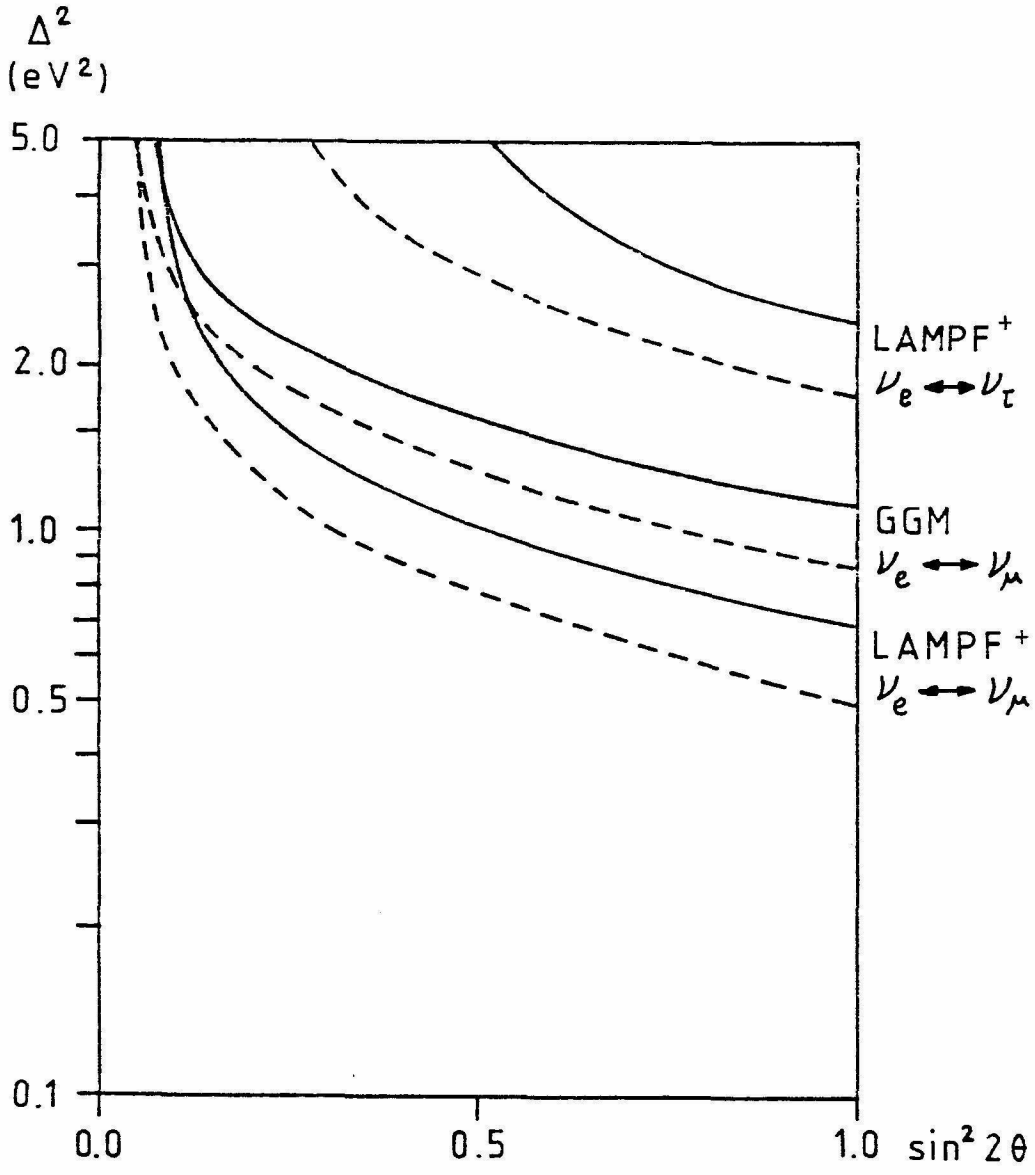

Fig. 1: The present limits on Δ^2 vs $\sin^2 2\theta$. The dashed and solid curves represent the confidence levels of 68%, and 90%, respectively. (Except for the solid line of GGM which is 95% c.l.). In each case the regions to the right of the curve can be excluded.

GGM: J. Blietschau et al., Nucl. Phys. B133, 205 (1978)

+LAMPF: P. Nemethy et al., contribution to Neutrino-80 Conference at Erice, Italy (1980)

CHAPTER 2

PHENOMENOLOGICAL MODEL FOR NEUTRINO OSCILLATIONS

In this chapter, a brief discussion on neutrino oscillations and the formalism which is relevant to the analysis of the experiment are presented.

Two neutrino mixing is considered explicitly here, because it is simple and provides a good starting point[17].

If neutrinos are massless, they cannot oscillate. As there is no experimental proof that neutrinos are massless, it will be assumed that they have masses. The consequences are investigated.

The physical neutrinos ν_e, ν_α ($\alpha=\mu,\tau...$) are created in weak-interaction processes. These weak eigenstates of neutrinos are not necessarily the pure mass eigenstates of the total Hamiltonian, ν_1, ν_2 (with masses m_1, m_2), but a linear combination thereof. This can be written as follows

$$\begin{pmatrix} \nu_e \\ \\ \nu_\alpha \end{pmatrix} = \begin{pmatrix} \cos\theta & \sin\theta \\ \\ -\sin\theta & \cos\theta \end{pmatrix} \begin{pmatrix} \nu_1 \\ \\ \nu_2 \end{pmatrix} .$$

Suppose a neutrino ν_e of energy E_ν is created at time t=0. The quantum mechanical state vector $|\Psi(0)>$ is described by $|\nu_e>$.

$$|\Psi(0)> = |\nu_e> .$$

At time t, the state vector is given by the expression,

$$|\Psi(t)\rangle = \exp(-iHt)\ |\Psi(0)\rangle$$
$$= \cos\theta|\nu_1\rangle\exp(-iE_1t) + \sin\theta|\nu_2\rangle\exp(-iE_2t)$$
since $H|\nu_i\rangle = E_i|\nu_i\rangle$
where $E_i = \sqrt{(p_i^2 + m_i^2)}$ $(\hbar = c = 1)$

and the neutrinos are assumed to be stable particles[18]. By grouping the coefficients, we have

$$|\Psi(t)\rangle = a(t)\ |\nu_e\rangle + b(t)|\nu_\alpha\rangle,$$
where $a(t) = \cos^2\theta\exp(-iE_1t) + \sin^2\theta\exp(-iE_2t)$
$b(t) = \cos\theta\sin\theta[\exp(-iE_1t) + \exp(-iE_2t)]$.

The probability to be in a $|\nu_e\rangle$ state at time t is given by

$$P(t) = |\langle\nu_e|\Psi(t)\rangle|^2 = |a(t)|^2 = 1 - \frac{1}{2}\sin^2 2\theta\ [1 - \cos(E_1-E_2)t] .$$

Assuming that $E_\nu \gg m_i$, which is of interest to us,

$$E_1 - E_2 \cong \frac{m_1^2 - m_2^2}{2E_\nu} , \text{ and}$$
$$P(t) = 1 - \frac{1}{2}\sin^2 2\theta[1-\cos(\frac{m_1^2-m_2^2}{2E_\nu})t] ,$$

or expressed in terms of distances from the source,

$$P(E_\nu, d, \Delta^2, \theta) = 1 - \frac{1}{2} \sin^2 2\theta \left[1-\cos\left(\frac{2.53\, d\Delta^2}{E_\nu}\right)\right],$$

where $\Delta^2 \equiv (m_1^2 - m_2^2)$ in eV^2

with d in meters

and E_ν in MeV.

The corresponding oscillation length is given by

$$\Lambda(\text{meters}) = \frac{2.48\, E_\nu(\text{MeV})}{\Delta^2\ (eV^2)} \quad .$$

The manifestations of the oscillation depend on the energy of the neutrino and the distance between source and detector. To detect neutrino oscillations, one has to measure the neutrino flux as a function of the energy, or the distance, or both.

Present experimental limits on Δ^2 and $\sin^2 2\theta$ for oscillations are shown in Fig. 1.

In the present experiments, oscillations of $\bar{\nu}_e \rightarrow$ anything ($\bar{\nu}_e \rightarrow \bar{\nu}_\mu$, $\bar{\nu}_e \rightarrow \nu_{eR}$, etc.) are investigated, using reactor antineutrinos. These antineutrinos have energies of a few MeV. For flight lengths of a few meters (8.79 m in this experiment), one can have a sensitivity for Δ^2 as low as 0.2 eV^2. This range is hard to explore with the more energetic accelerator neutrinos. Reactor experiments thus play important and unique roles.

CHAPTER 3

EXPERIMENTAL METHOD

In this chapter, the antineutrino source, the antineutrino detection reaction, the experimental set-up, the data acquisition and data reduction are discussed.The measurement of the detector efficiency is also presented.

The inverse beta decay of the neutron, $\bar{\nu}_e + p \rightarrow e^+ + n$[19], which has a relatively large cross section among reactor neutrino induced reactions, is used as the detection reaction. The cross section is given by,

$$\sigma(E_\nu)=(9.13\pm0.11)\cdot(E_\nu-1.293)\sqrt{(E_\nu-1.293)^2-(0.511)^2}\ \times10^{-44}\ cm^2.$$

(E_ν in units of MeV).
A derivation of the cross section is given in Appendix A. The error on the cross section is due to the uncertainty of the neutron lifetime.

The energy spectrum of the positrons is measured. (The positron energy will always mean the positron kinetic energy.) From energy-momentum conservation, the positron carries away most of the energy of the incoming neutrino. Therefore the energy of the positron is simply related to the energy of the neutrino by $E_{e+} = E_\nu - E_o$. E_o is the reaction threshold given by $E_o = (m_n - m_p) + m_e = 1.804$ MeV.

As a result, the positron energy spectrum conveys the information of the neutrino spectrum, and a deviation of the measured positron spectrum from the expected one (with no oscillation), will indicate

oscillations. The expected positron spectrum is the neutrino spectrum folded with the cross section and the detector efficiencies (see Section 3.4). The neutrino spectrum can be calculated, or can be obtained from the inversion of the beta spectrum of uranium-235 fission products.

For this purpose, the detector was designed with emphasis on good positron energy resolution, low background, and high detection efficiency. The effect of oscillations would be washed out with poor energy resolution. Since the expected counting rate is low (<2 c/h), low background and high detection efficiency are essential.

3.1. THE ILL REACTOR AS A SOURCE OF ELECTRON ANTINEUTRINOS

The experiment was carried out at the High Flux Reactor of the Institut Laue-Langevin (ILL), at Grenoble, France. The reactor has 57 MW thermal power. The fuel element of the reactor consists of 8.5 kg of 93% enriched ^{235}U in the form of UAl_3. This almost pure ^{235}U core has the advantage of lending itself to a well defined prediction of the electron antineutrino spectrum. For each fission of ^{235}U, in a 30 days period, 5.3 electron antineutrinos are emitted as a result of beta decays of the fission fragments. The measured energy released per fission (not including the antineutrino energy) is (198.4 ± 1.7 MeV[20]). Thus the ILL reactor constitutes a source strength of 9.5×10^{18} electron antineutrinos per second.

The reactor core is a cylinder, 40 cm in diameter and 80 cm in height. This small "point-like" core, compared with the core of a power reactor which is as big as several meters, makes the ILL reactor ideal

to study oscillations at small distances from the source.

The operating cycle of the reactor consists of 40 days of reactor-on followed by 10 days of reactor-off. The reactor-off periods were used to measure the background.

At present, there are two different calculations for the reactor antineutrino spectrum. One is by Davis et al. (DV)[21] and the other one is by Avignone and Greenwood (AG)[22], as shown in Fig. 2. These antineutrino spectra are calculated from a catalogue of all fission fragments. There are about 710 fission products, of which about 200 have complete experimentally determined decay schemes. The problem of this method is the treatment of the remaining 510 "unknowns" which have short lifetimes and correspondingly large Q-values for the beta decay. These "unknowns" are treated differently by the two calculations. As a result there is a discrepancy between the two predictions, DV lying about 30% below AG in the energy region of interest to us (2.8 MeV to 10 MeV). The uncertainty in the antineutrino spectrum is conservatively claimed by DV to be from 10% at 2 MeV up to 30% at 8 MeV antineutrino energy.

Another method to obtain the antineutrino spectrum is by measuring the electron spectrum from ^{235}U fission and converting it to the antineutrino spectrum. The electron spectrum measured recently at ILL[23] using an on-line magnetic beta-spectrometer is in good agreement with the prediction by DV. The shape of the electron spectrum is verified to $\pm 2\%$. The normalization is also in excellent agreement, with a systematic error of less than 10%. An electron spectrum measurement at the Oak Ridge

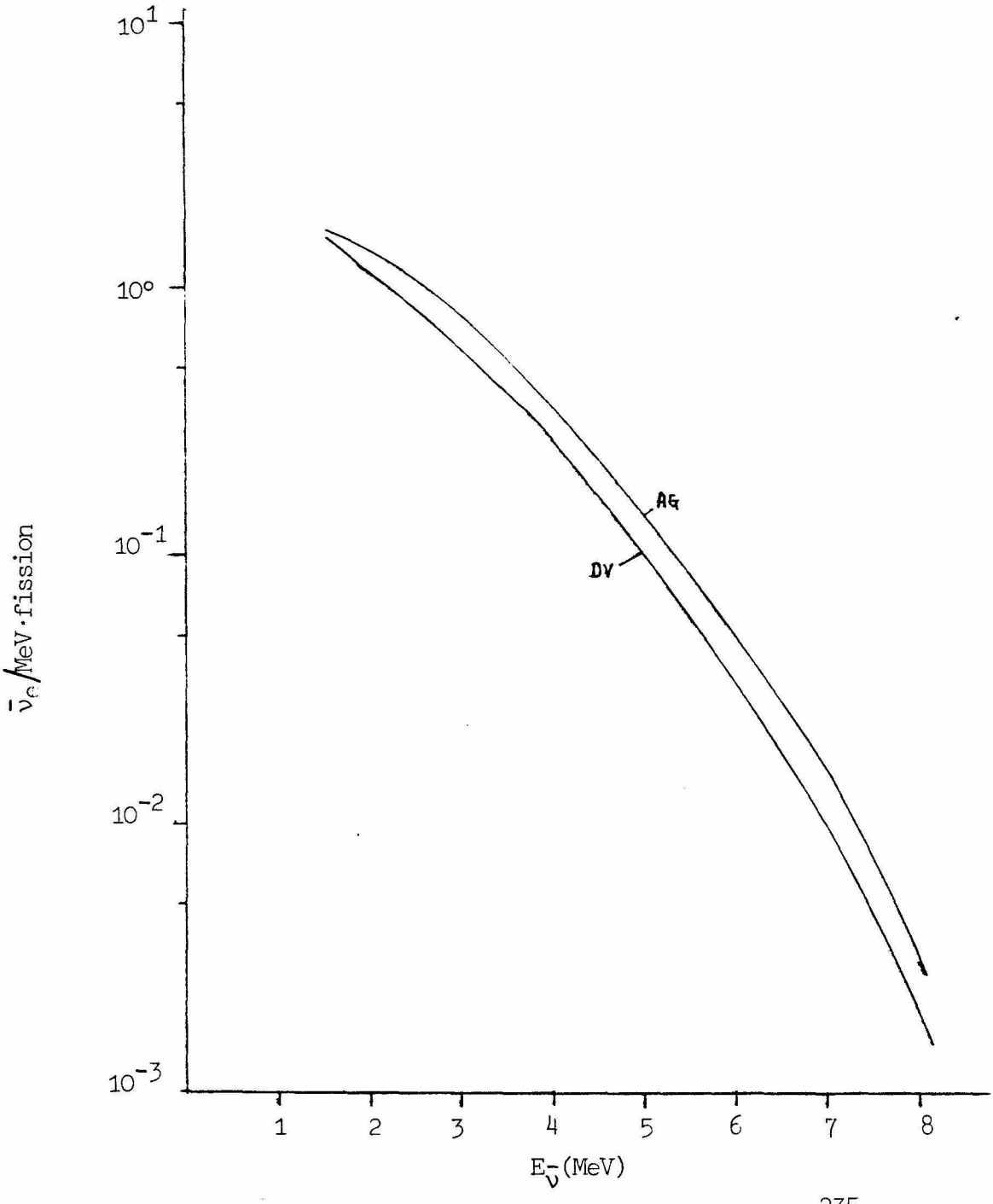

Fig. 2: Energy spectrum of antineutrinos from ^{235}U - see text for explanation.

reactor[24] also tends to favor DV. Therefore, the antineutrino spectrum is assumed to be the DV spectrum with 10% error on the normalization.

The antineutrinos emerging from the beta decays of the surrounding material activated by the neutrons, have low energies. In the case of the ILL reactor, the core is made out of aluminum which can emit antineutrinos with a maximum energy of 2.8 MeV. Since only events with $E_{e+} > 1$ MeV (i.e., $E_{\bar{\nu}} > 2.8$ MeV) are accepted in this experiment, antineutrinos below 2.8 MeV are of no importance. About 16% of the fission-product antineutrinos have energies more than 2.8 MeV.

The antineutrino flux at the detector is given by,

$$\phi(E_{\bar{\nu}},d) = \frac{S \cdot N(E_{\bar{\nu}})}{4\pi d^2} ,$$

where $S=1.80 \times 10^{18}$ is the number of fissions per second in the ILL reactor, $N(E_{\bar{\nu}})$ is the antineutrino spectrum calculated by DV, and d=8.76m is the distance from the source to the detector averaged over the detector and the core size.

3.2. DETECTION REACTION

The detector is set up at 8.76 m (antineutrino flux of $9.8 \times 10^{11} cm^{-2} sec^{-1}$) from the reactor core in the basement of the reactor building (Fig. 3). The detector is a multilayer sandwich of five liquid scintillator planes and four ^3He wire counter planes as shown in Fig. 4.

A schematic representation of the detection reaction is shown in Fig. 5. The antineutrino interacts with a proton of the liquid

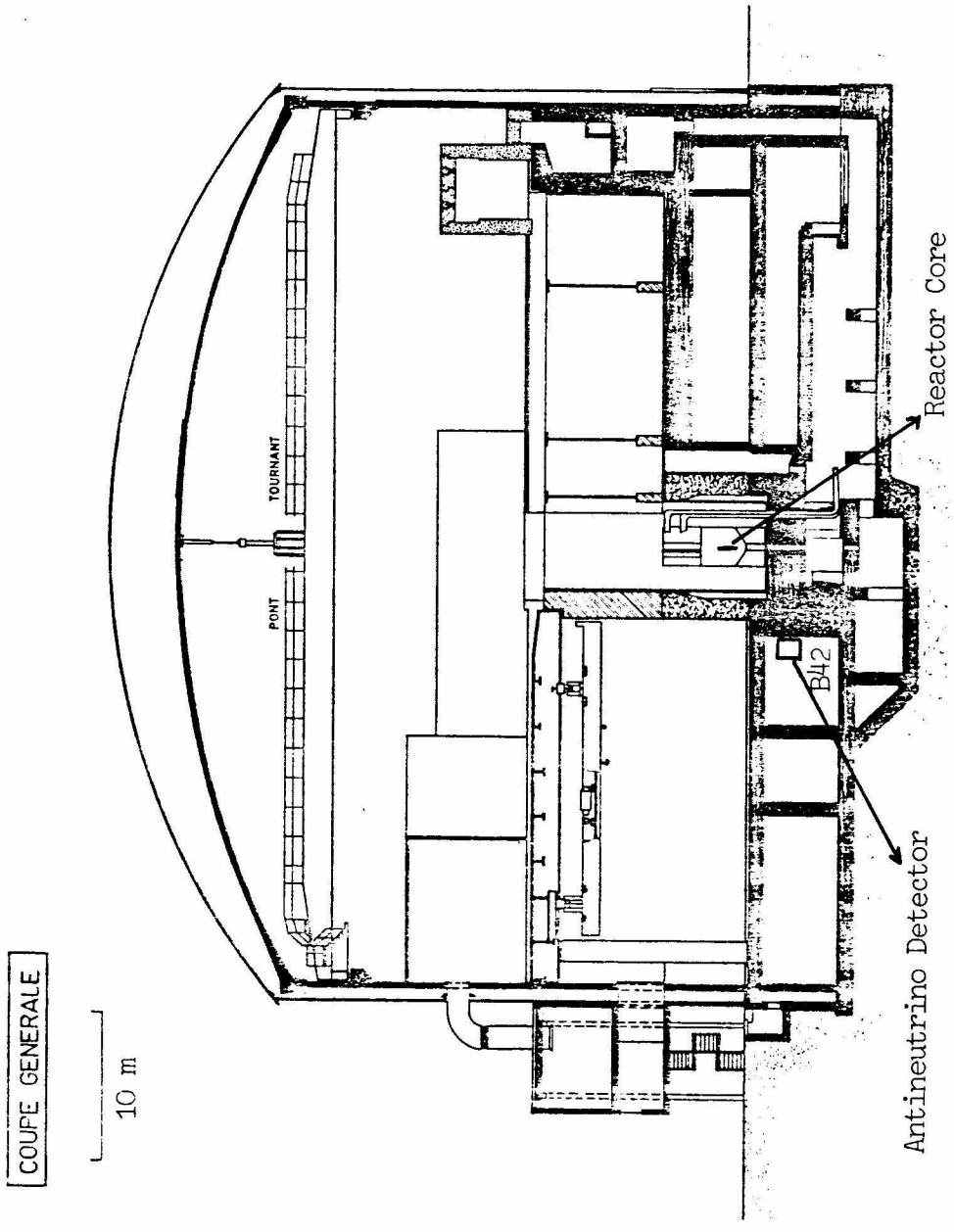

Fig. 3: Vertical Section of the ILL Reactor

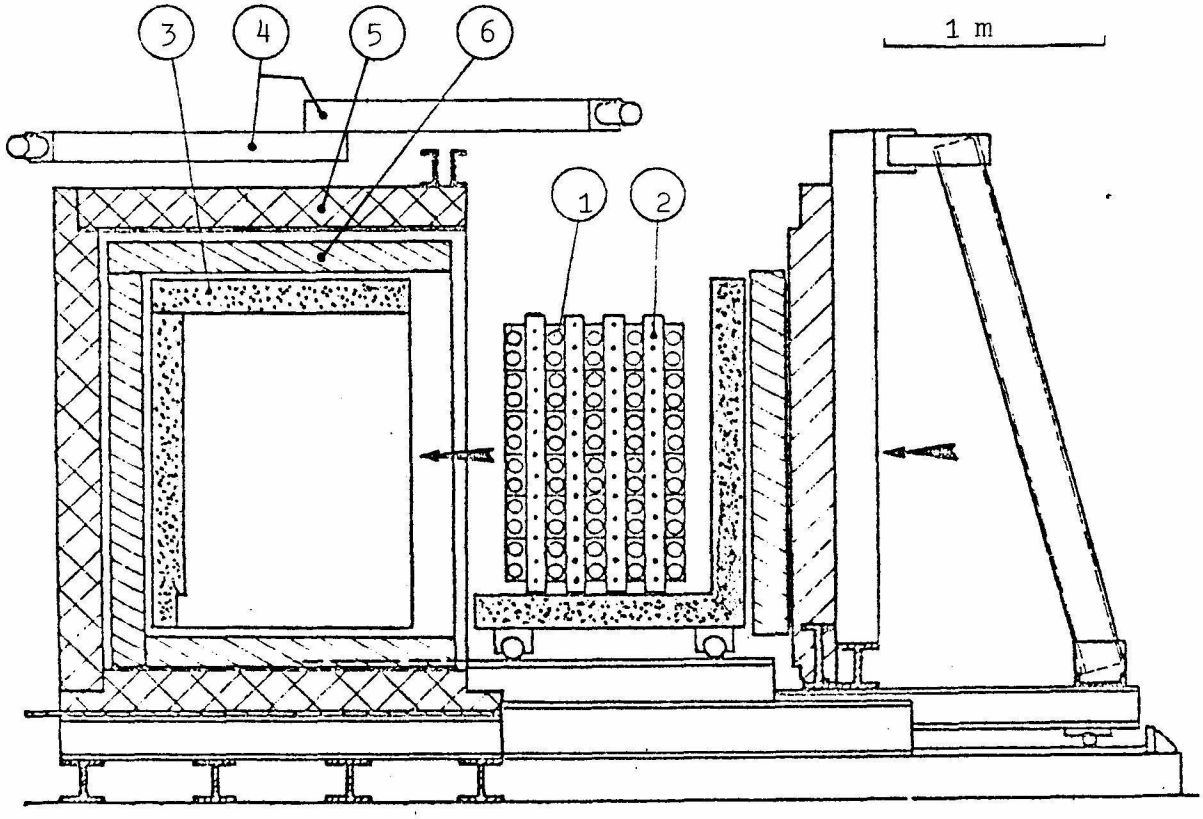

Fig. 4: Detector Assembly showing:

1) target cell
2) ^{3}He counter
3) veto tank
4) umbrella
5) lead house
6) polyethylene

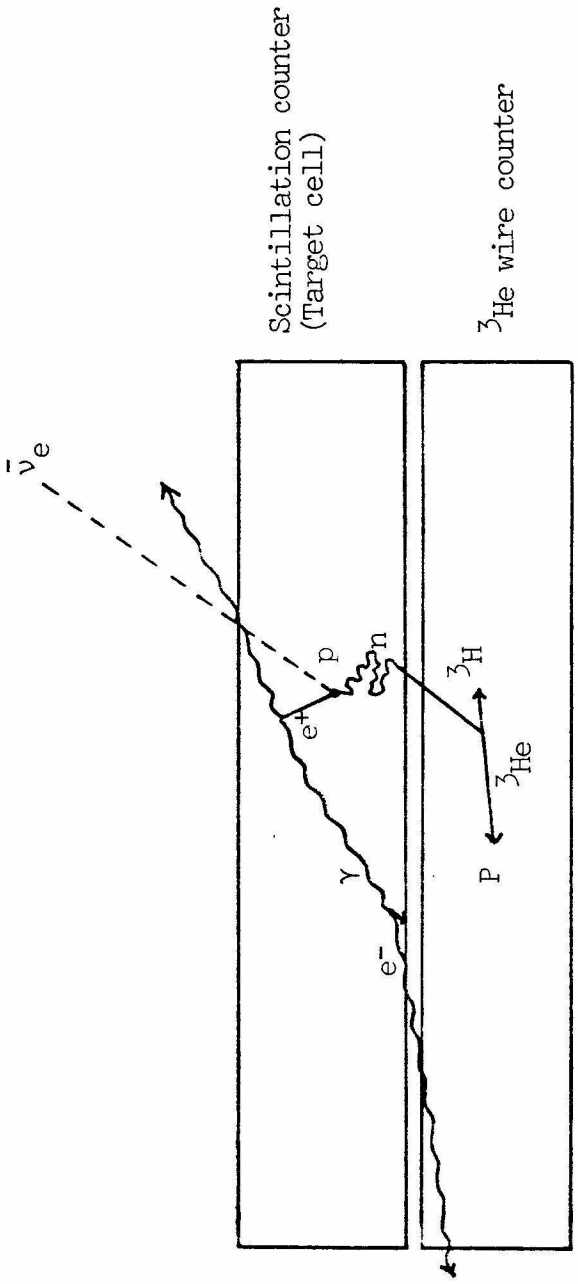

Fig. 5: Schematic representation of the $\bar{\nu}_e + p \rightarrow e^+ + n$ reaction.

scintillator in the target cell, making a positron and a neutron.

The positron slows down by ionization in the liquid scintillator producing a prompt light pulse. The scintillation light output is proportional to the energy of the positron. Upon stopping, the positron annihilates into two 0.511 MeV gamma rays. Most of the annihilation gamma rays escape from the target cell, since their mean free path is 14 cm in the liquid scintillator. A hardware threshold was set at about 0.85 MeV and no attempt was made to detect these coincidence annihilation gamma rays.

The neutron (typically 10 keV), does not make a pulse in the liquid scintillator. Instead, it is thermalized in the target cell within a few μs and diffuses into the ^{3}He counter with a mean diffusion time of about 150 μs. The neutron is captured in a ^{3}He counter via the reaction $n+^{3}He \rightarrow p+^{3}H+765$ keV. ^{3}He is chosen because it has a large neutron capture cross section (5500 barns for a thermal neutron varying as the inverse of its velocity), and because it is insensitive to gamma rays due to the small number of electrons in the ^{3}He. Both the p and ^{3}H are detected by the ^{3}He counter which operates in the proportional region.

A delayed coincidence between the target cell and the ^{3}He counter is the signature of a good event.

BACKGROUND CONSIDERATIONS

The background which gives rise to false events is divided into two parts: reactor associated and reactor independent. Each is further

divided into an accidental component and a time-correlated component, within the delayed coincidence time window. Accidentals are the product of the singles rates in the target cells and in the ^{3}He counters, multiplied by the coincidence time window.

The reactor associated background is due to the gamma rays and the neutrons with energies up to 10 MeV from the reactor core and its surroundings. It is an unpleasant source of background and was eliminated in this experiment by means of massive shielding.

The reactor-independent background is measured during the reactor-off periods. Nevertheless, great care is taken to minimize it. The shielding helps to keep it low. The most serious background comes from neutrons created by cosmic-ray induced events. Fast and slow neutrons are created by the nucleonic and the muonic component of the cosmic rays. The nucleonic component is mostly eliminated by the concrete shielding above the detector. The remaining muonic component, which creates slow and fast neutrons, is suppressed by the anticoincidence veto system. The mechanisms for the production of neutrons by the cosmic-ray muons are nuclear disintegration (scattering), photonuclear process (bremsstrahlung) and stopped-muon capture by the nuclei.

Accidentals due to the radioactivity of the detectors are hard to remove, so care is taken to minimize natural radioactivities.

One particularly dangerous background is a time-correlated event due to single fast neutrons. A fast neutron can make a recoil proton

pulse in the target cell. The neutron subsequently thermalizes in the target cell and is captured in a ^{3}He counter. This simulates an antineutrino event. To suppress this background, a pulse shape discrimination (PSD) technique[25] is used for the target cell events. Certain scintillators give different pulse shapes for electrons and for protons, because their ionization densities are different. By looking at the shape of these pulses, one can distinguish whether the initiating event is a gamma ray (recoil electron) or a neutron (recoil proton).

3.3. DETECTOR SYSTEM

Details of each detector component with its performances are described below.

TARGET CELLS

The 30 target cells are arranged in five vertical planes of six cells in each plane. Each target cell has an outside dimension of 9cm x 20cm x 88cm, and is made out of 6mm lucite (Fig. 6). The thickness of the cell is chosen so that it is thick enough for neutron thermalization, yet sufficiently thin to prevent excessive neutron absorption by the protons.

As a scintillant, a mineral oil based proton rich liquid scintillator NE235C, specially developed by Nuclear Enterprises [26], is used. The total volume of the scintillator liquid is 377 ℓ corresponding to 2.39×10^{28} protons. This scintillator is a modified version of NE235H with additional pulse shape properties, which enables one to use the PSD technique. (As far as the PSD is concerned, NE213 is by far the

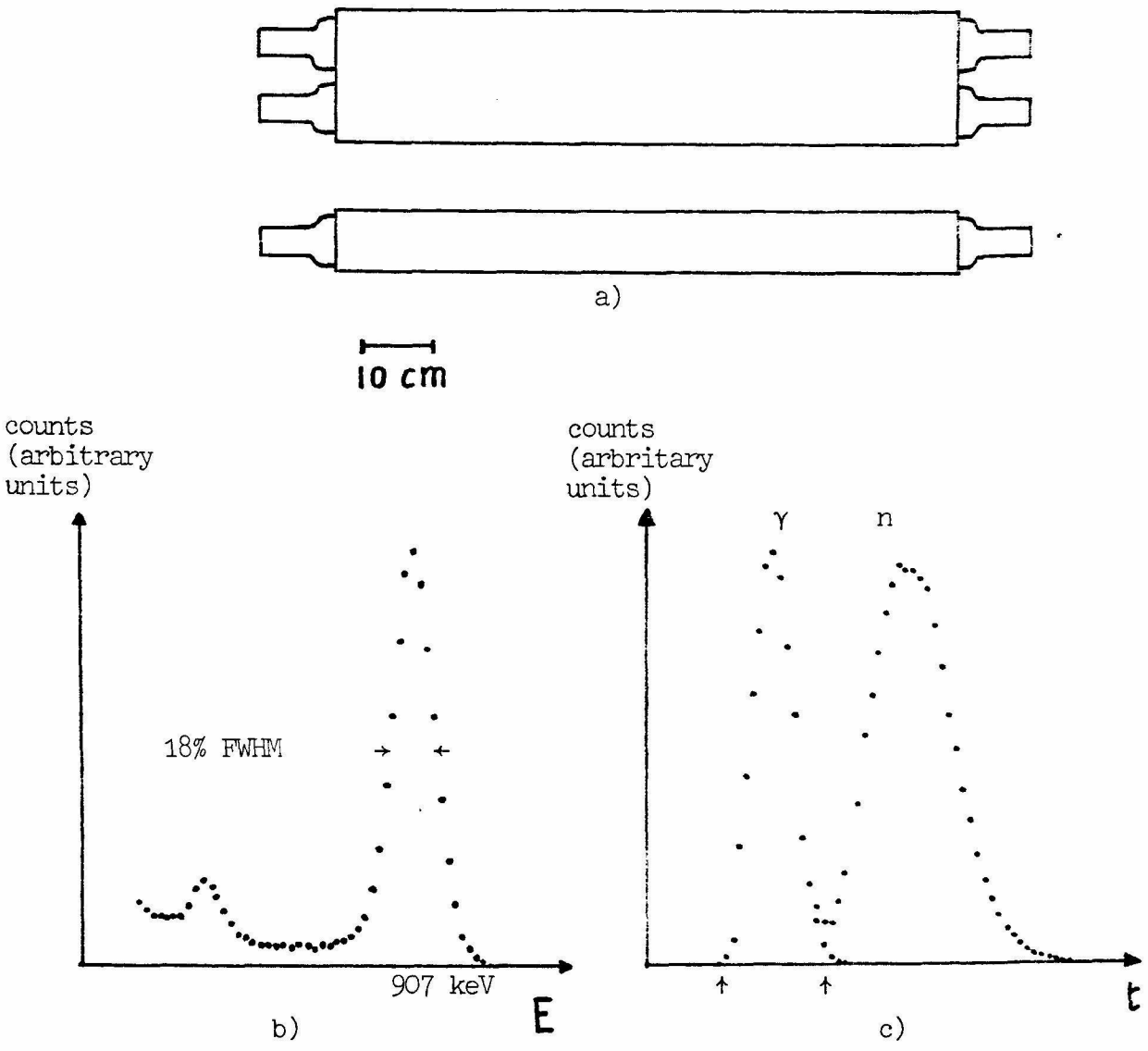

Fig. 6: Target cell and the performances

a) The side and top view of a target cell with photomultiplier tubes

b) The energy spectrum from a ^{65}Zn source

c) The PSD spectrum for 1 MeV electron equivalent
The arrows indicate the PSD window used in the analysis.

best scintillator. But since it attacks the lucite, has a poor H/C ratio and poor light transmission, and also is very expensive, NE235C was chosen.) NE235C has an H/C ratio of 1.72 ± 0.015 and a density of 0.861 g/cm^3. Its light output is 61.5% that of anthracene and the light transmission length is better than 3 meters.

The PSD performance of the NE235C is compared with that of NE213 in Fig. 7. The test was performed with each liquid in a 5cm x 5cm circular cylindrical glass vessel which is optically coupled to a 5 cm photomultiplier tube (Amperex XP2230). An Am-Be source was used as a neutron source.

After each target cell was filled with NE235C, pure nitrogen gas was bubbled through the liquid to remove the dissolved oxygen. The oxygen acts as a quenching material in the scintillant which reduces the light output and degrades the PSD performance. Total internal reflection at the air-lucite interface of the target-cell walls provides the light collection. Each target cell is viewed at each end by two optically coupled 7.5 cm Amperex XP2312 photomultiplier tubes. The XP2312 tube is a high gain, fast timing, low dark current tube. The remaining area of the end surfaces are covered by diffuse reflectors with an air gap for maximum light output[27]. Each cell is wrapped with aluminized paper to further enhance the light collection.

The target cell energy resolution is 18% FWHM at 1 MeV, with an exellent homogeneity (Fig. 6). The measurement was done with a single-line gamma-ray source with forward-scattered Compton electrons. The

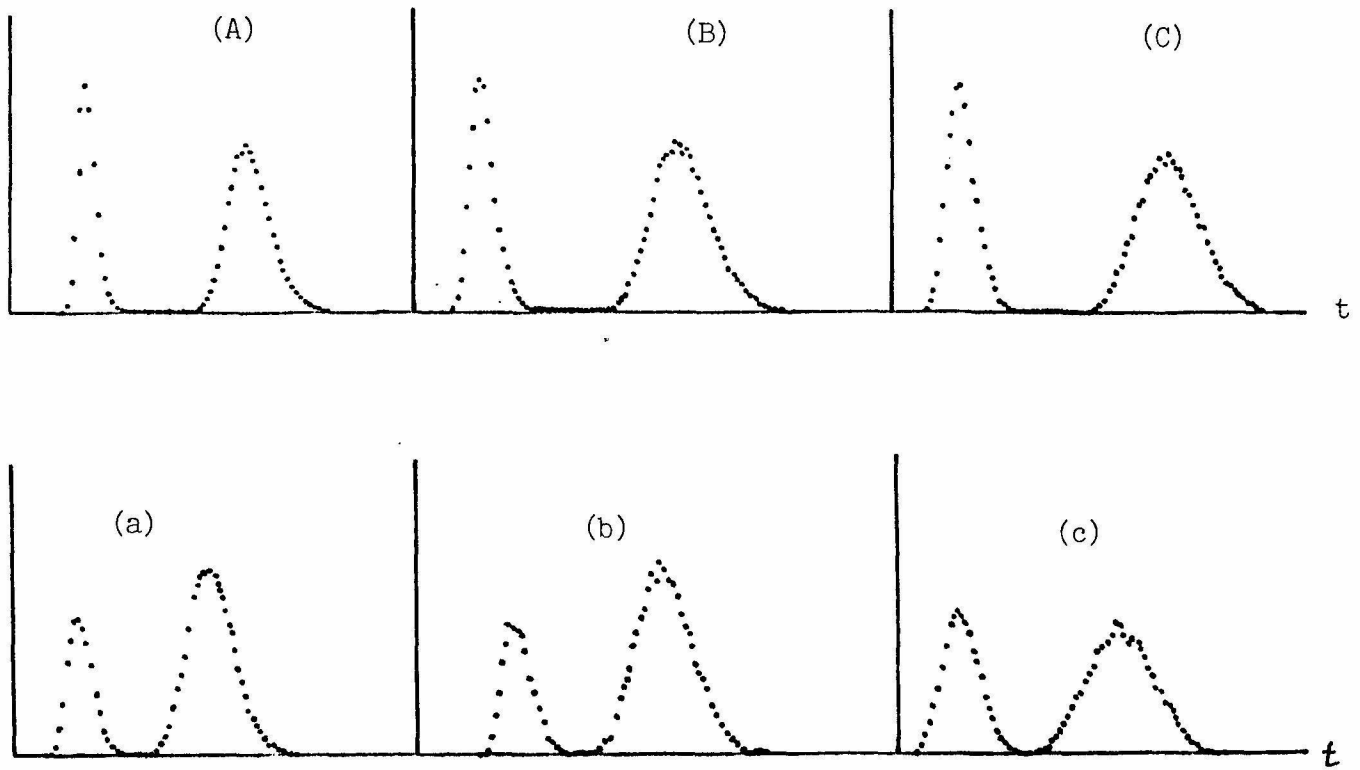

Fig. 7: PSD performances of NE213 (A,B,C) and NE235C (a,b,c)
The energy windows are 0.9-1.1 MeV (A,a), 0.5-0.8 MeV (B,b),
0.2 - 0.5 MeV (C,c), respectively. The time calibration is 0.53 ns/ch.
The vertical axes are counts in arbitrary unit.

energy of the Compton electrons is then well defined. The backscattered gamma rays were detected with a NaI detector in coincidence with the target cell.

The absolute energy calibration was done using the same method with the 4.42 MeV gamma rays from the exited $^{12}C^*$ from the Am-Be source ($\alpha + Be \rightarrow n + {}^{12}C^*$). Its error is less than 2%.

The PSD property of the target cells is shown in Fig. 6. The energy dependence of the PSD is such that the two peaks become somewhat narrower and closer with higher energies. The valley of the PSD shifts slightly toward the gamma (electron) peak as the energy gets larger. This effect is corrected for in the analysis. The high energy neutron background is reduced by a factor 50 with this PSD cut.

HELIUM-3 WIRE COUNTERS

Four large ^3He wire chambers, each with an outside dimension of 8cm x 88cm x 126cm, were built. The counters, each containing 75 liters of ^3He gas at atmospheric pressure, are sandwiched between the target planes (Fig. 4). Special care was taken to choose materials with low natural radioactivities. The box has a frame made from stainless steel. The windows are 0.2 mm steel sheets. A single stainless steel wire of 50 microns diameter is threaded through the chamber with a spacing of 2 cm. The counters were carefully outgassed before filling. They were sealed after being filled up with ^3He gas. No degradation of the chambers has been seen after 9 months of operation.

The energy spectra of the ^{3}He counters are shown in Fig. 8. The energy resolution at 765 keV (full energy peak) is about 25% FWHM for the best counter. The shoulder at the low energy side is due to the wall effect. The smallest possible signal of detection is 190 keV where the triton is accompanied by an escape proton. A hardwire threshold is set at around 185 keV. The actual window used in the analysis is between 275 keV and 1340 keV. The background of each counter due to natural radioactivity is about 0.75 counts min^{-1} in this window.

VETO TANKS

The assembly of the target cells and of the ^{3}He counters is completely surrounded by six mechanically and optically independent liquid scintillator planes, arranged in such a fashion that the radiation leaks between plane boundaries are less than 9 mm wide (detailed drawings are shown in the appendix C). Each tank, made out of aluminum, is slightly different from the others but all are 12 cm thick. The tanks are filled with the liquid scintillator NE235H. Each tank is provided with light reflectors. The reflectors on the large surface are lucite panels sealed on the edges to an aluminum sheet, thus taking advantage of the total reflection of the lucite-air interface. Two adjacent edges are fitted with aluminum sheets coated with TiO_2 paint and sealed with thin lucite sheets. The two other edges have lucite windows. The scintillation light is collected from the lucite windows by wavelength shifter bars[27), 28)] coupled to two 7.5 cm photomultiplier tubes (Amperex XP2312). The wavelength shifter bars are acrylic bars (16mm thick) with 2 mg/l of BBQ concentration. When such a bar is placed against the

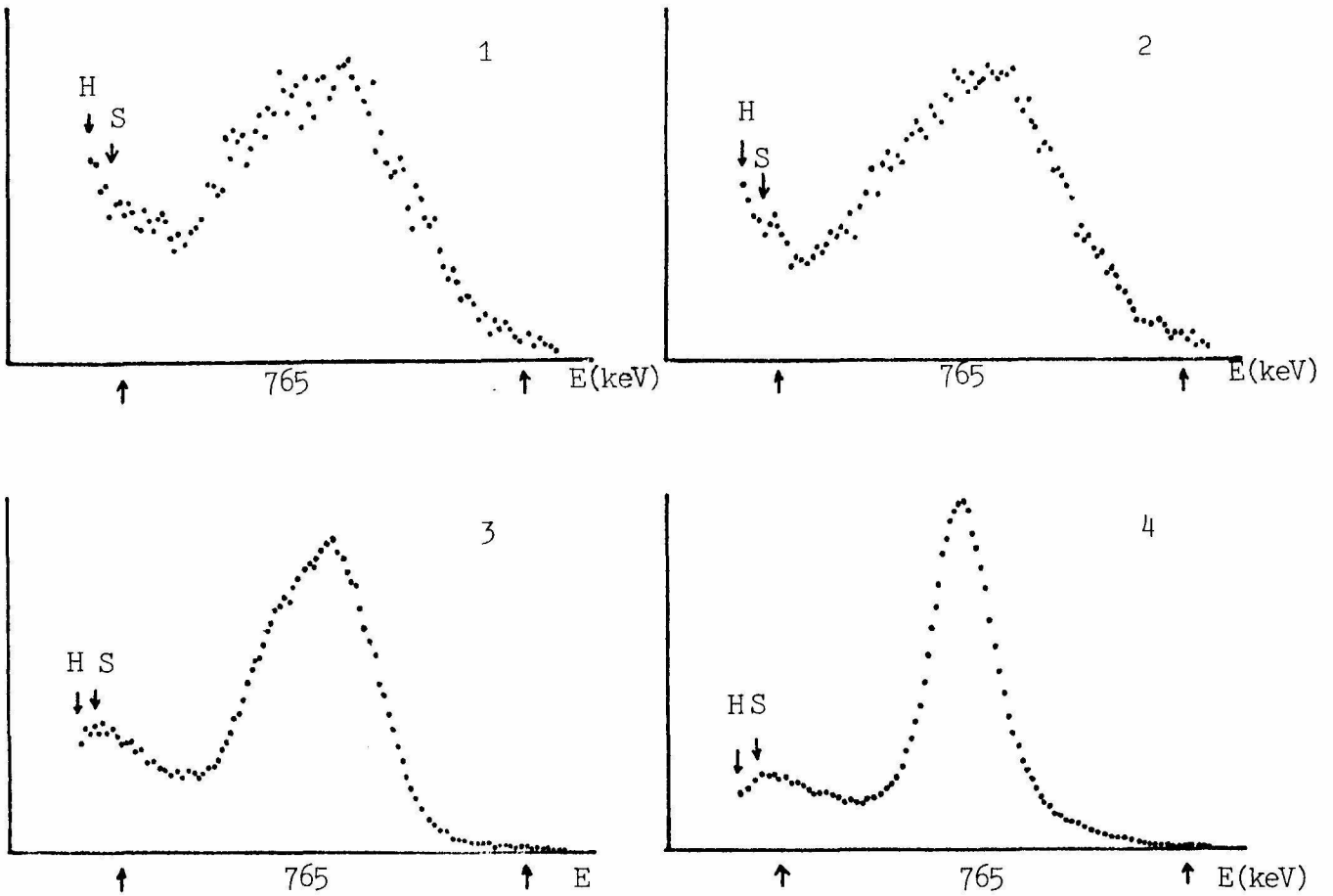

Fig. 8: The Energy Spectra of the ^{3}He counters. For the detector positions, see Fig. B.1. The hardware threshold is shown by the arrows (↓) with H. The software threshold set by a data aquisition program is shown by the arrow (↓) with S. The energy window used in the analysis is shown by the arrow (↑). The vertical axes are counts in arbitrary unit.

edge of the scintillation counter, the blue scintillation light is absorbed in it and reemitted as isotropic green light which propagates by total internal reflection to the end of the bar where it is collected by the photomultiplier tubes.

The six veto tanks are mounted on their movable transport system, rolling on a pair of demountable tracks. The vertical front veto tank is attached to the horizontal bottom tank and constitutes a movable unit on which the target cells and the ^{3}He counters are installed, while the other four veto tanks form the second unit (Fig. 4).

The energy spectrum of the cosmic muon through-peak of the top veto tank is shown in Fig. 9. The hardware threshold (indicated by an arrow) is set so that the efficiency of the veto tanks in detecting cosmic muons is better than 99.8%.

The electronics for the veto tank pulse generates a 320 μs signal (Long Veto). ^{3}He events in coincidence with this signal are rejected. This 320 μs interval is a compromise between good neutron rejection (it is about 95% efficient) and low dead time (about 8%). A 10 μs signal is also generated for the anticoincidence with the target cell events. It reduces the target cell count rates above 2.5 MeV by a factor of 80.

UMBRELLAS

Four additional cosmic ray veto scintillation counters are installed on top of the lead house (Fig. 4). They serve to suppress the cosmic-ray muon related events where muons are stopped in the top part of the lead house and also to suppress the bremsstrahlung by electrons

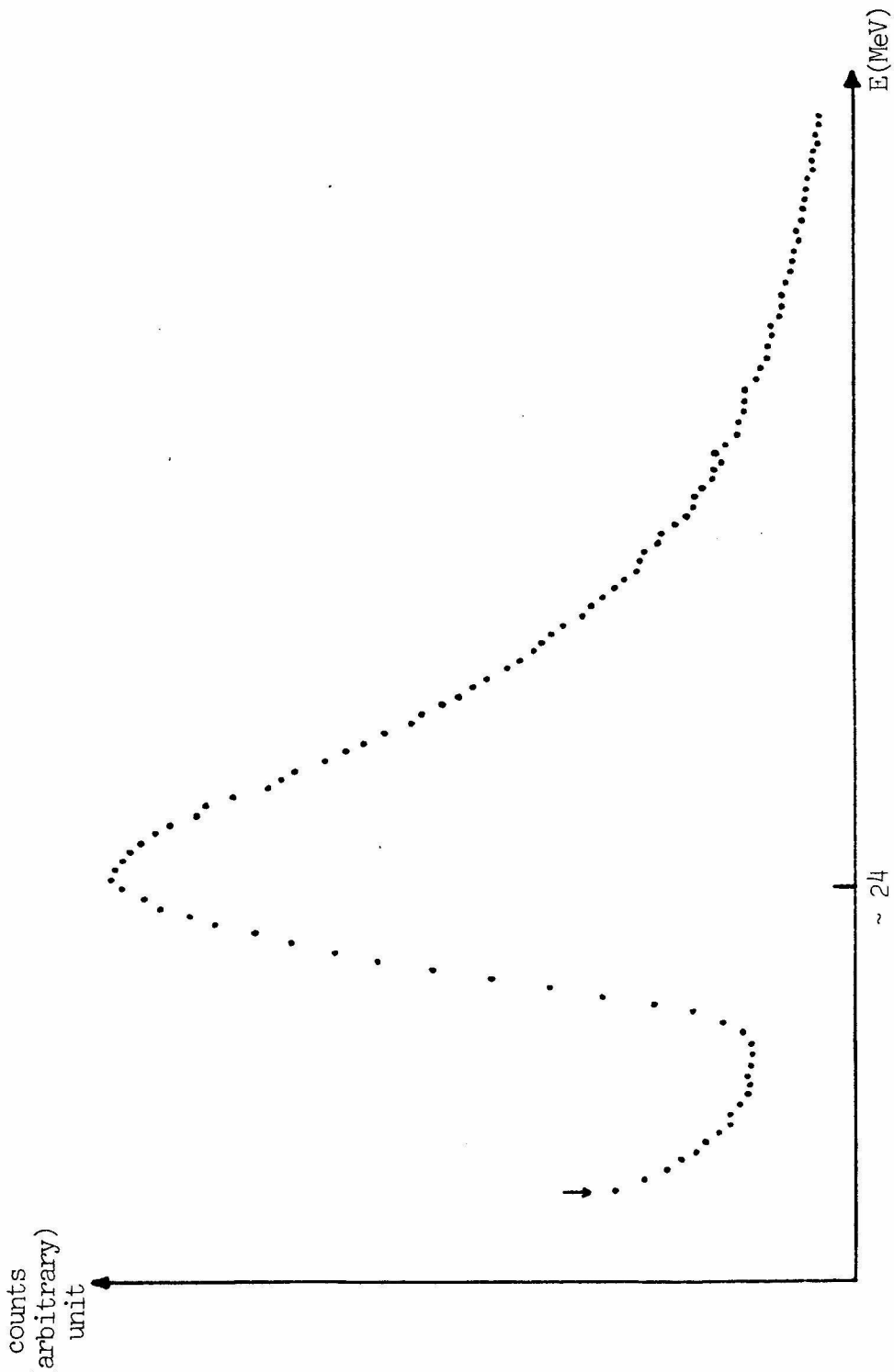

Fig. 9: Energy spectrum of the cosmic-muon through-peak for the top veto tank. The arrow indicates the hardware threshold.

from the decay of stopped muons in the lead. Each one has 8 cm (thickness) x 130 cm x 150 cm outside dimension, is made out of 6 mm thick lucite, and contains NE235H. The wavelength shifter bars are placed on two sides of the counter, while TiO_2 painted reflectors are provided with an air gap on two other sides. A 12.5 cm tube (Amperex XP1040) is used to view the bars. Each photomultiplier tube is shielded with a mu metal sheet to screen out stray magnetic fields.

A 10 μs signal is generated by the vetos and the umbrellas, and is used as an anticoincidence with the target cell events. This cuts down fast neutron events in the target cells by a factor of 2. In addition to the veto rejection, it further reduces the gamma-ray rates above 2 MeV by 15%.

Details of the effects of these veto anticoincidences are discussed at the section 3.6.

SHIELDING

A 20 cm thick lead shield is used, based on a measurement of the gamma-ray activities at the experimental site. The measurement was done with a 7.5 cm NaI crystal inside a small lead house. The gamma-ray spectrum was measured as a function of the thickness of the lead. No variation was seen by varying the thickness from 15 cm to 20 cm. Special low background lead was obtained and used for the inner part of the construction. A selection for low background was made for the remaining parts with normal lead. The lead is supported by steel frames outside and 2 cm steel plates inside. The 20 ton lead door moves on rollers

and rails, so as to allow open access to the veto house (Fig. 4).

Inside the steel house, 15 cm thick polyethelene is used (Fig. 4) to moderate and capture neutrons. The 12 cm thick veto tanks serve as additional absorbers.

During the early test runs, it was observed that a high flux of thermal neutrons was entering through the right side of the ceiling of the room. These slow neutrons were captured in the lead and the steel giving rise to high energy gamma rays, some of which in turn were detected by the target cells although not at a rate that could significantly affect the accidental background. It was observed that these slow neutrons did not increase the ^{3}He singles rates and, as it turned out later, the coincidence rates.

Additional sheets of B_4C were added outside the lead house and a 50 cm thick concrete wall was built on the right side of the lead house. This additional shielding is sufficient to make the target cell rates reactor independent. Since the shielding did not reduce the coincidence rate, it is concluded that there is no reactor associated time correlated background.

A 2.5 m concrete shield is placed above the detector. Along with the concrete of the reactor shield, it eliminates most of the nucleonic component and attenuates the muonic component.

MISCELLANEOUS

Pressurized air is blown continuously into the veto house to keep out any radioactivity, essentially the 1.29 MeV gamma rays of

^{41}Ar from the reactor, in the air surrounding the detector.

This pressurized air, by passing through a copper coil immersed in a refrigerant at constant temperature, also serves to remove the heat generated by the photomultiplier tube bases and by the preamplifiers of the ^{3}He counters. As a result, the temperature of the detector system is maintained to $\pm$ 0.5°C for each run.

3.4 EFFICIENCY OF THE DETECTOR

The efficiency of the detector is the product of the positron detection efficiency and the neutron detection efficiency,

$$\varepsilon_{TOT} = \varepsilon_n(t)\varepsilon_{e^+} \cdot$$

The neutron detection efficiency $\varepsilon_n(t)$ depends on the delayed coincidence time window t. The positron detection efficiency $\varepsilon_{e^+} = \eta(E_{e^+})A(PSD)$ is the efficiency $\eta(E_{e^+})$ corrected for the acceptance of the PSD window.

The positron yield is then,

$$Y(E_e^+) = N_p\phi(E_{\bar{\nu}},d)\sigma(E_{\bar{\nu}})\varepsilon_{TOT}$$

where N_p is the number of target protons, $\phi(E_{\bar{\nu}},d)$ is the antineutrino spectrum at the detector, $\sigma(E_{\bar{\nu}})$ is the $\bar{\nu}_e p \rightarrow e^+ n$ cross section, with $E_e^+ = E_{\bar{\nu}} - 1.8$ (MeV).

a) Neutron Detection Efficiency

The neutron detection efficiency was measured using MeV neutrons from an Am-Be source and keV neutrons from a Sb-Be source. It was also

calculated using a neutron transport computer program[29].

With the Am-Be source, the neutrons have enough energy to make signals in the target cells. One counts the single neutron events in the target cell identified as such by the PSD, and coincidence rates of a target cell and the adjacent ^{3}He counters. The ratio of the two gives the efficiency. After adding a 1.0% correction, which is calculated by the neutron transport program, to correct for the difference between fast and slow neutrons, $\varepsilon_n(t=\infty) = 26.5 \pm 2.0\%$ was ditermined.

A spectrum of the time distribution between a fast neutron prompt pulse in the target cell and a delayed pulse in the ^{3}He counter is shown in Fig. 10. This also shows the timing characteristic of the $\bar{\nu}_e p \rightarrow e^+ n$ reaction, since slow and fast neutrons take a similar time for thermalization.

A 200 μs time window for the delayed coincidence, which has a 81% acceptance, is used in the analysis as explained in section 3.6.

The neutron efficiency within this time window then becomes $\varepsilon_n(200\ \mu s) = 21.5 \pm 1.6\%$.

The Sb-Be neutron source is a calibrated ($\pm$ 3%) standard source[30] emitting 1.639×10^3 neutrons per second at 12:00 GMT on Jan. 29, 1979. Its neutrons have energies of about 20 keV which is comparable to the neutrons from the inverse beta decay. The mean life of the source is 60.20 ± 0.03 days[31]. The source strength during the efficiency measurement was 7.58 neutrons per second at the beginning and 7.05 neutrons per second at the end. This variation of the source strength with time

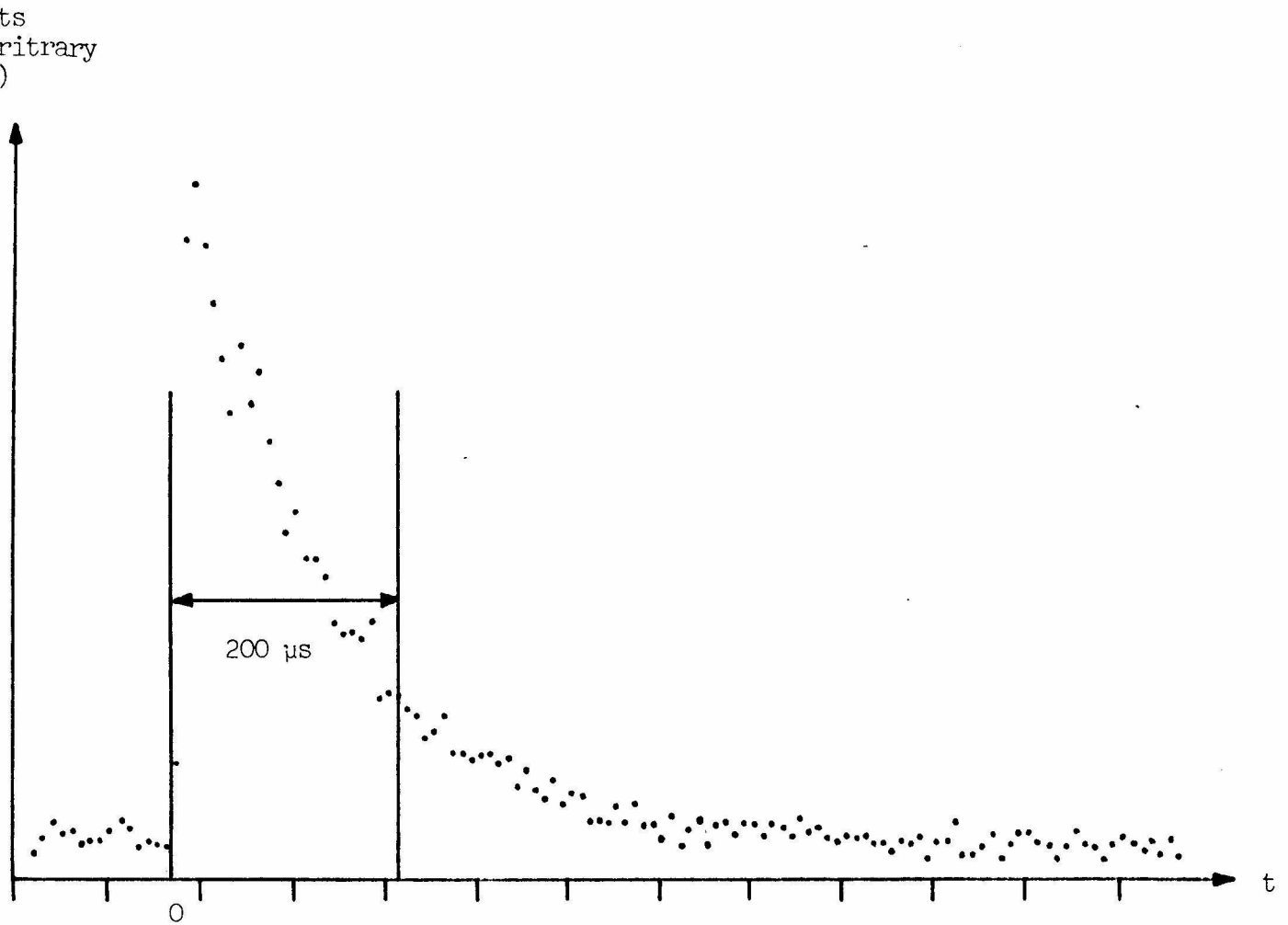

Fig. 10: The prompt target-delayed ^{3}He timing spectrum of fast neutrons. The entire range is 1024 μs. There is an offset of 128 μs. The 200 μs time window is used in the analysis.

is taken into account in the calculation. Compared to the source strength, the accidental background (0.03 per second) was negligible.

The active dimensions of the source are 4 mm (dia.) x 4 mm (long) encapsulated in a stainless steel cylinder of 6.6 mm (dia.) x 10.1 mm (long.). The neutron source was put into a specially built target cell. The source was moved in 3 dimensions, with a 1 mm precision using stepping motors. 56 different source positions and three target cell positions were mapped (see Fig. B.1 in appendix B). Each point was measured to about 2% statistical error.

As the absolute source strength is known, the ratio of the ^{3}He rate divided by the source strength gives the neutron detection efficiency.

Because of the high gamma-ray flux from this source, the software threshold was set higher than in the analysis. The resulting correction was measured using an Am-Li source in various positions. This relative correction, which varies between 12% and 15%, was applied in the efficiency calculation.

The variation of the efficiency along the 9 cm target cell width, using one ^{3}He counter only, is shown in Fig. 11. As can be seen from the figure, the efficiency varies linearly with the width. For the central target cells, the neutron can be detected in the ^{3}He counter on either side, and the contribution from each side has to be summed. Then the efficiency becomes a constant over the whole width. Only a small fraction (less than 0.5%) of the neutrons will end up in a

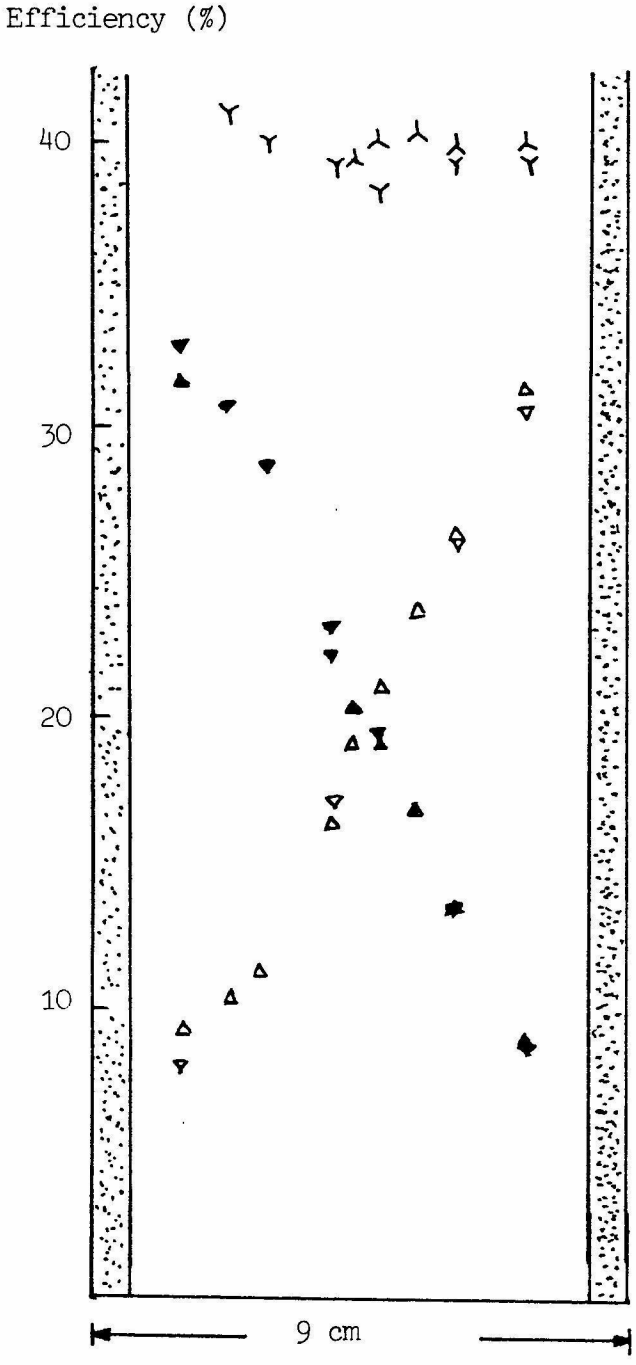

Fig. 11: The variation of the neutron detection efficiency along the target cell width showing:

▲: efficiency for the left ^{3}He counter

Δ: efficiency for the right ^{3}He counter

Y: the sum of the left and right.

The lucite walls are illustrated as a dotted area.

non-adjacent ^{3}He counter. The dependence of the efficiency on the 20 cm height and the 88 cm length of the target cell are shown in Fig. 12. The efficiency remains constant over a wide range and drops off at the edge.

The overall neutron detection efficiency, within the 200 μs coincidence time window and in the ^{3}He energy window, was determined to be

$$\varepsilon_n(200\ \mu s) = 20.2 \pm 1.7\%.$$

Detailed calculations are provided in appendix B.

b) The Positron Detection Efficiency

The positron detection efficiency $\eta(E_{e^+})$ was calculated with a Monte-Carlo program. The positron yield without the $\eta(E_{e^+})$ correction, $N_p \phi(E_\nu) \varepsilon_n(T) A(PSD)$, is shown as a dotted line in Fig. 13. The acceptance A(PSD) of the PSD window used in the final analysis is 97%. Using this raw spectrum, the program calculates the deformation $\eta(E_{e^+})$ due to the effect of the finite range of the positron, the 0.511 MeV annihilation gamma rays , the energy resolution of the detector, and the anti-neutrinos interacting in the lucite. The resulting positron spectrum, $Y(E_{e^+})$, is shown with a solid line in Fig. 13. The distortion is not very significant.

3.5. DATA ACQUISITION

a) Electronics

A diagram of the electronic scheme is shown in Fig. 14. It consists of circuits for the target cells, the ^{3}He counters, the vetos

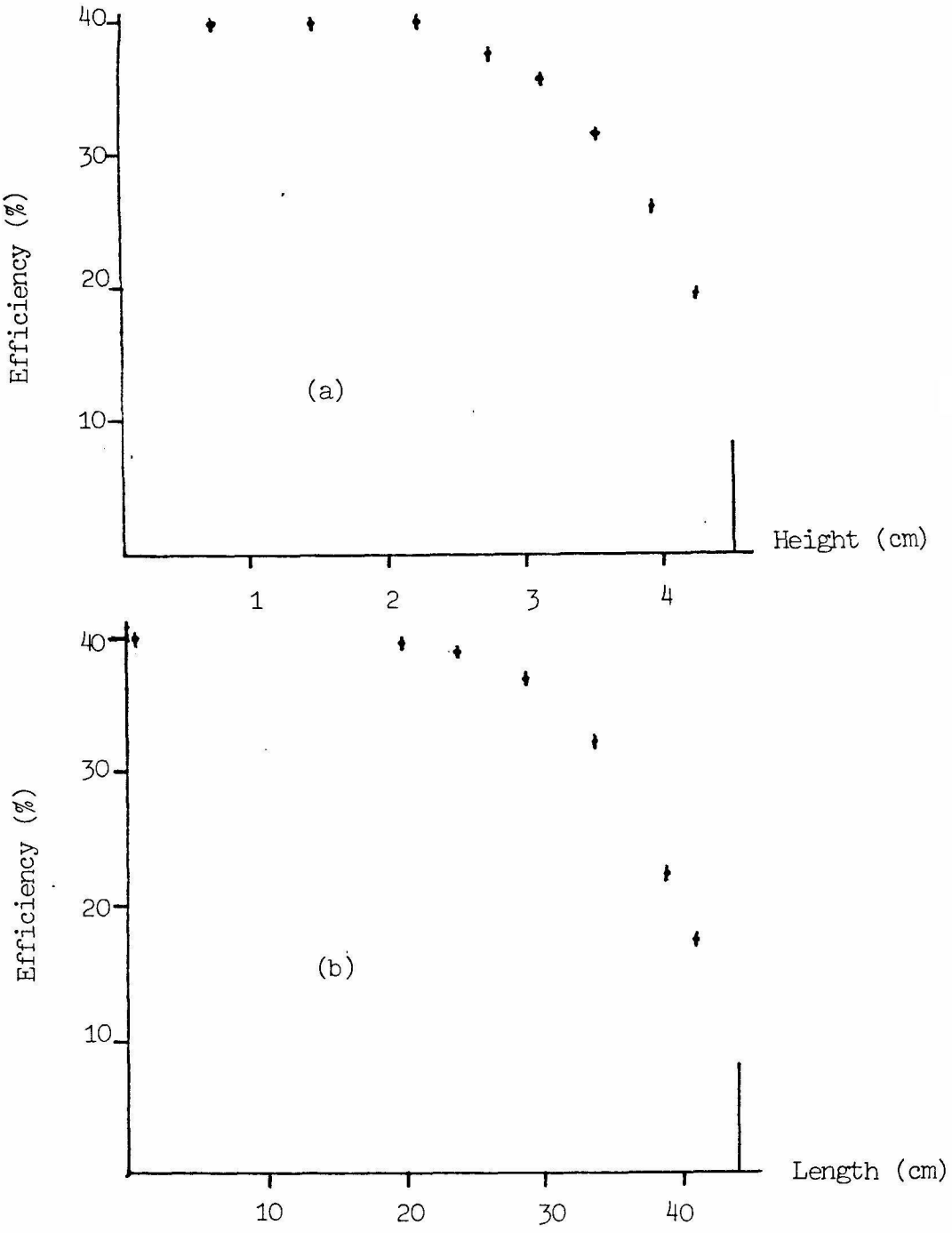

Fig. 12: Variation of the neutron detection efficiency along the target cell height (a) and the length (b) using the ^{3}He counters on both sides. The zero positions in the horizontal axes represent the center of the target cell.

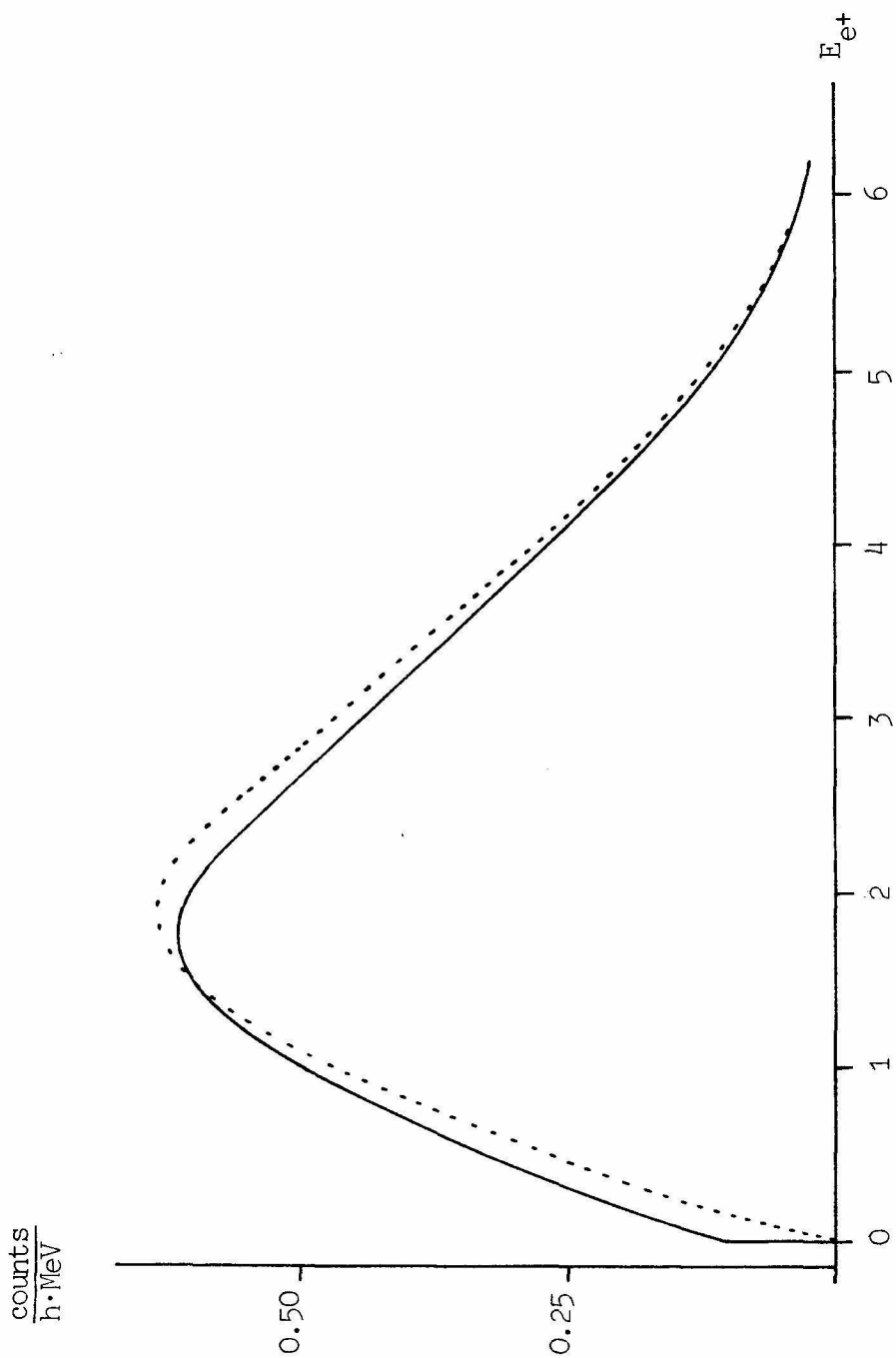

Fig. 13: The positron energy spectra before (dotted curve) and after (solid curve) the positron detection efficiency $\eta(E_{e^+})$ correction.

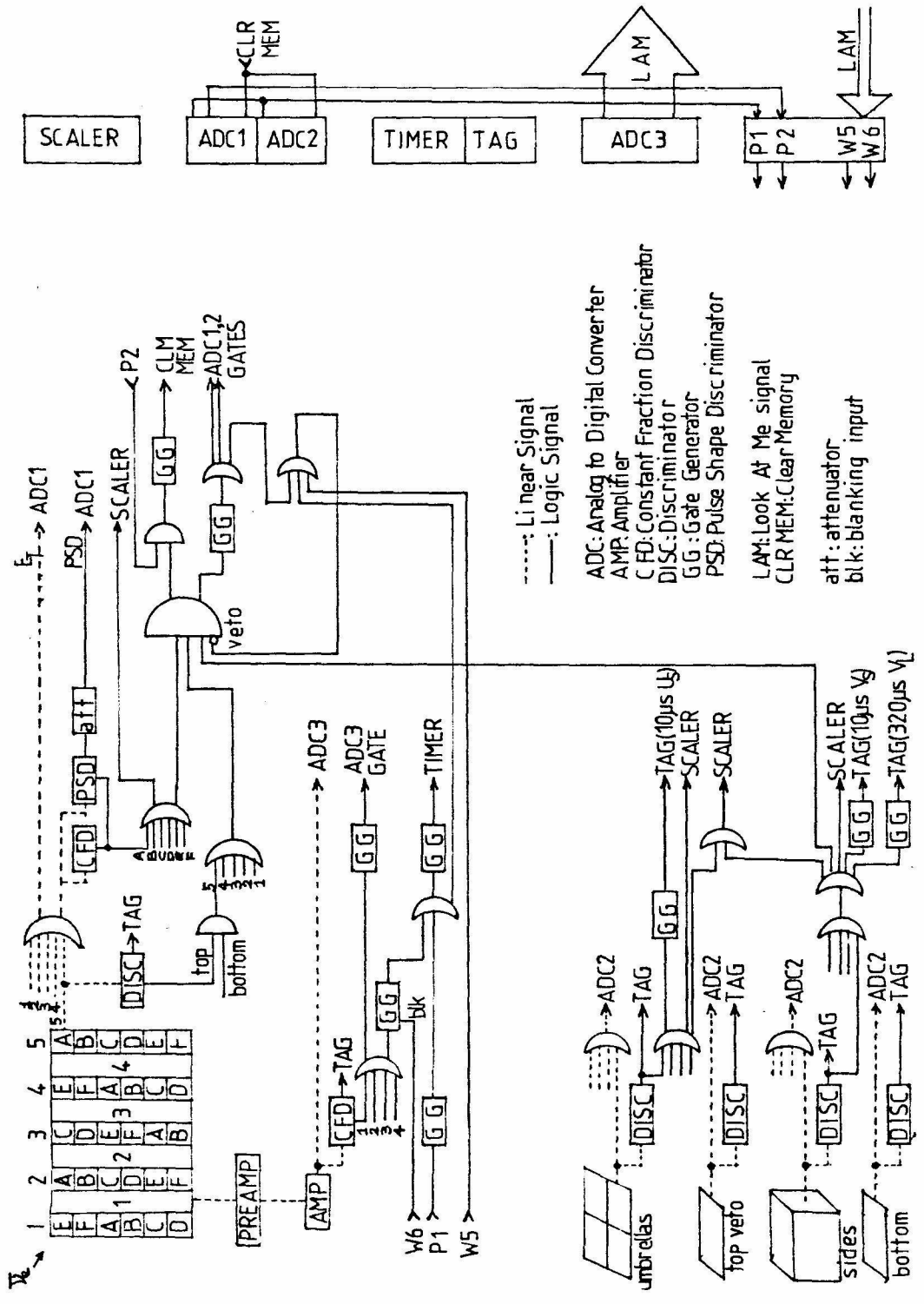

Fig. 14: The electronics diagram

and the umbrellas. The analyzed signals enter the CAMAC system which communicates with a PDP 11/40 computer. Data are stored in the computer memory by an on-line program and also written on magnetic tapes for final off-line analysis.

TARGET CELL CIRCUITS

The signals from the four photomultiplier tubes of each target cell are passively added together. The 30 target cells are arranged into 6 groups (A to F in Fig. 14) and into 5 planes (1 to 5 in Fig. 14). Signals from the same group but different planes are fanned-in together (to reduce the number of electronic modules). The particular way of fanning-in avoids a possible accumulation of the 0.511 MeV annihilation gamma rays in adjacent target cells. The energy and the PSD signals from the target cells are analyzed by the ADC (Analog to Digital Converter). The 12 channel ADC of 9 bits is charge sensitive with 9 μs of digitization time. The digitized signals of each channel are incrementally stored in its own 32 word buffered memory. When the memory is full, it is cleared and a new sequence begins.

Each signal from a target cell above the hardware threshold sets a bit in a TAG unit, and records the time in a TIMER unit. Both the TAG and the TIMER unit have 32 word memories which cycle continuously and synchronously with the target cell ADC. Thus the time and the TAG pattern of the previous target cell events are always available.

The TAG unit has 48 bits (30 for the target cells, 4 for the ^{3}He counters, 6 for the veto tanks, 4 for the umbrellas, and 3 special veto

bits, one being unused), which identify the detector modules. With the TIMER and the TAG informations, an event can be reconstructed when and where it occurred.

^{3}HE COUNTER CIRCUIT

The signals from each ^{3}He counter are preamplified, amplified, and then analyzed in the ^{3}He ADC (peak sensing, 11 bits), with each counter having its own channel. The ^{3}He signals set a bit in the TAG, and record the time in the TIMER. They also generate a LAM("look-at-me") in the CAMAC system.

VETO CIRCUITS

Each veto or umbrella pulse above the hardware threshold sets a bit in the TAG. However, this does not cause the TAG memory to increment. The energies of the vetos and the umbrellas are analyzed in their own ADC, but are not used in the normal data acquisition mode. They are used in the calibration of the vetos and umbrellas, along with the TAG information.

The cosmic-ray anticoincidences are not hardwired. Instead, three special bits are provided in the TAG unit for the vetos and the umbrellas. A veto tank signal above the hardware threshold generates a short veto signal (10 μs) and a long veto signal (320 μs) which are set at the input of the identification TAG. In the same manner, an umbrella event generates a short umbrella signal (10 μs). The corresponding special veto bits are set in the TAG memory, whenever a target cell event or a ^{3}He event occurs while these signals are on.These special veto bits are

used for the anticoincidences in the analysis.

With the electronics set-up described above, the data acquisition works as follows:

1) A signal from a ^{3}He counter above the hardware threshold (set just above the noise level indicated by arrows in Fig. 8) generates a LAM signal to the CAMAC, which triggers a computer interrupt. The time, the TAG, and the energy of the ^{3}He event are read into the computer.

2) If the ^{3}He event is above the software energy threshold, the information from 3 preceding target cell events is then read and stored into the computer memory. The idea is that by using the second and the third previous events, the accidental background can be measured "on-line". It also gives a possibility to study the stability of the system and the correlated background.

3) Data are written on a magnetic tape for the off-line analysis. The on-line program monitors the system and analyzes the data while the experiment is running.

An "event" consists of a ^{3}He event with 3 previous target cell events. The raw data recorded on the tapes are: the time, the TAG, the energy of a ^{3}He counter, the times, TAGS, energies and PSDS of three previous target cell events.

The rate of "events" is about 25 min^{-1}. With this rate, a 2400 feet magnetic tape is filled in 3 days. This time period constitutes a "run". Between the two runs, system checks are made as described below.

b) Experimental Procedures

After each tape is filled, an Am-Be source is inserted inside the lead house for the energy calibrations of the detector. The Compton edge of the 4.43 MeV gamma ray from $^{12}C^{*}$ is used to check the gain of the each target cell. If necessary the gain was reset to the nominal value by adjusting the high voltage of the respective phototube. Simultaneously the neutrons from the Am-Be source are used for the calibration of each ^{3}He counter.

The vetos and umbrellas are calibrated with the cosmic-ray muon through-peak.

Various singles rates of the detector components are monitored with the on-line program during the measurements, and are shown in Table 1. It should be noted that the singles rates of the target cells and the ^{3}He counters are essentially reactor independent.

The stability of the detectors and the electronics was found to be excellent (Section 3.6b). During the calibrations, it was observed that the gain shift of the target cells was less than 1%.

2338.91 hours (real time) of reactor-on data and 970.27 hours (real time) of reactor-off data were collected.

Dead time was measured, using a pulser, to be 15% and 20% for reactor off and on respectively. The difference is due to the high rate of the umbrellas when the reactor is on.

Reactor Status	count rates (counts/sec)			
	30 target cells^{+}	4 ^{3}He counters*	6 veto tanks^{+}	4 umbrellas^{+}
OFF	216.3	.422	256.8	440
ON	216.7	.427	258.6	5384

+ : counts above the hardware threshold

$*$: counts above the software threshold ("event" rates)

Table 1. The count rates of the detector components sampled before and during the full power operation of the reactor.

3.6. DATA REDUCTION

a) Selection of the Good Events

The mean time interval between the target cell singles events is 4.5 ms (at a target cell singles rates of 220 sec^{-1}), whereas the time interval of the neutrino event is about 200 μs (Fig. 10). Consequently, only the first target cell event preceding the ^3He event is considered to be a candidate for a neutrino event.

Various conditions are imposed to suppress backgrounds originating from various sources. The selection of the good events is made as follows:

1) Reject the first previous target cell event if it occurred in more than one cell. This is meant to reject cosmic-ray related events and a possible Compton scattering of high energy bremsstrahlung.

2) Reject a multi ^3He event since there is only one neutron created by a neutrino event. These events are rare (0.05 c/min).

3) Reject a ^3He event outside the energy window, to suppress the gamma-ray background and the electronic noise at low energy and the alpha background at high energy. This condition reduces the total ^3He counting rate from 25 counts min^{-1} (the rate of the data acquisition) to 11 counts min^{-1}. Most of the eliminated events are due to alpha activity in the ^3He counters.

4) Reject a ^3He event occurring in a plane not adjacent to the plane of the first previous target cell event. This condition cuts down the accidental background by a factor of 2.5 which can be seen from a geometrical argument. The reason that this condition can be imposed is that

the neutrons created in the reaction cannot travel far without being absorbed. The probability that the neutron crosses another target plane and is detected by the next ^{3}He counter is very small (less than 0.5%).

5) Reject a ^{3}He event which is in coincidence with the long veto (320 μs). It rejects the neutrons, created in the shielding and in the detector by cosmic rays, which diffuse into the system. It cuts the total ^{3}He counting rate from 11 min^{-1} to 4 min^{-1}.

6) Reject the first previous target cell event in coincidence with a short veto or a short umbrella signal (10 μs). It suppresses the bremsstrahlung events caused by decay electrons of cosmic muons stopped in the shielding. For correlated neutron-gamma ray events, it overlaps with the long veto rejection. In addition, owing to the umbrellas alone, it reduces the fast neutron rate by a factor of 2.

7) Reject a ^{3}He event which comes more than 200 μs after the target cell event. This is the time window used in the analysis which accepts 81% of the neutrino induced events. This window is a compromise between good efficiency and signal to background ratio. A 300 μs window will accept 94% of the events but the accidental background will increase 50%, in proportion to the time window.

8) Reject an event if the two previous target cell events are separated by less than 300 μs. This condition was first imposed since it would not be known which of the two is the positron event. It was found later that this condition reduces the background below 2 MeV by a factor of 2. From the study of the double and the triple target cell events in coincidence with a ^{3}He event, the energy spectrum of those rejected events shows a Compton edge around 2.2 MeV from neutron capture on protons.

These events are caused presumably by multiple neutron events created by cosmic rays in the shielding. For example, two neutrons are captured by protons in the target cells making 2.2 MeV gamma rays while a third one enters the ^{3}He counter.

9) Reject neutron (recoil proton) events of the first previous target cell events using the PSD. As the valley of the PSD slightly depends on the energy, the PSD spectrum of each target cell is fitted as a function of the energy and shifted accordingly to bring the valleys to the same position independently of the energy. The PSD cut is made such that the acceptance of the positron event, A(PSD), is 97%.

The rejection efficiency of some of the important cuts are shown in Table 2.

After imposing the conditions 1)-8), a two dimensional energy-PSD spectrum is constructed from the data. The PSD spectra for several energy regions are shown in Fig. 15. The areas under the neutron peak are the same for reactor-on and reactor-off demonstrating that there are no reactor associated fast neutrons, whereas the area under the gamma (electron or positron) peak is clearly enhanced for reactor-on owing to antineutrino events.

The energy spectra for reactor-on and reactor-off are obtained by rejecting the events under the neutron peak (condition 9), and are shown in Fig. 16. These spectra are dead time corrected. Clearly,there is a signal associated with the reactor. It will be shown in the following that this reactor associated signal is indeed a neutrino induced positron signal.

	Rejection Conditions				Dead time(%)	Gamma - rays				neutrons
	adj.	T_{12}	V_L	U_S		1.0-1.3 MeV	1.3-2.2 MeV	2.2-4.2 MeV	4.2-8.8 MeV	1.0-8.8 MeV
Reactor-off 715.516 hrs. real time	1	1	1	1	15.0	0.84±0.04	1.05±0.04	0.47±0.03	0.31±0.02	4.60±0.09
	1	1	1	0	14.5	0.94±0.04	1.20±0.04	0.65±0.03	0.44±0.03	6.85±0.11
	1	1	0	1	6.7	1.16±0.04	1.66±0.05	0.59±0.03	0.37±0.02	4.47±0.08
	1	0	1	1	8.4	1.07±0.04	1.55±0.05	0.57±0.03	0.38±0.02	4.50±0.08
	0	1	1	1	15.0	1.93±0.06	2.07±0.06	0.83±0.04	0.47±0.03	5.59±0.10
Reactor-on 843.55 hrs. real time	1	1	1	1	20.0	1.04±0.04	1.54±0.05	1.20±0.04	0.43±0.03	4.65±0.08
	1	1	1	0	15.0	1.10±0.04	1.68±0.05	1.34±0.04	0.56±0.03	7.08±0.10
	1	1	0	1	11.7	1.38±0.04	2.16±0.05	1.29±0.04	0.46±0.03	4.52±0.08
	1	0	1	1	13.4	1.29±0.04	2.12±0.05	1.30±0.04	0.49±0.03	4.54±0.08

Table 2: The rejection efficiencies of various cuts. The dead time corrected rates are in units of c/hr. The rejection conditions are shown by 1 (imposed) or 0(relaxed). The symbols are:

adj: adjacency requirement, condition 4) in the text

T_{12}: 300 μs veto for target cell events, condition 8) in the text

V_L : 320 μs long veto for ^{3}He events, condition 5) in the text

U_S : 10 μs short umbrella only for taget cell events, condition 6) in the text.

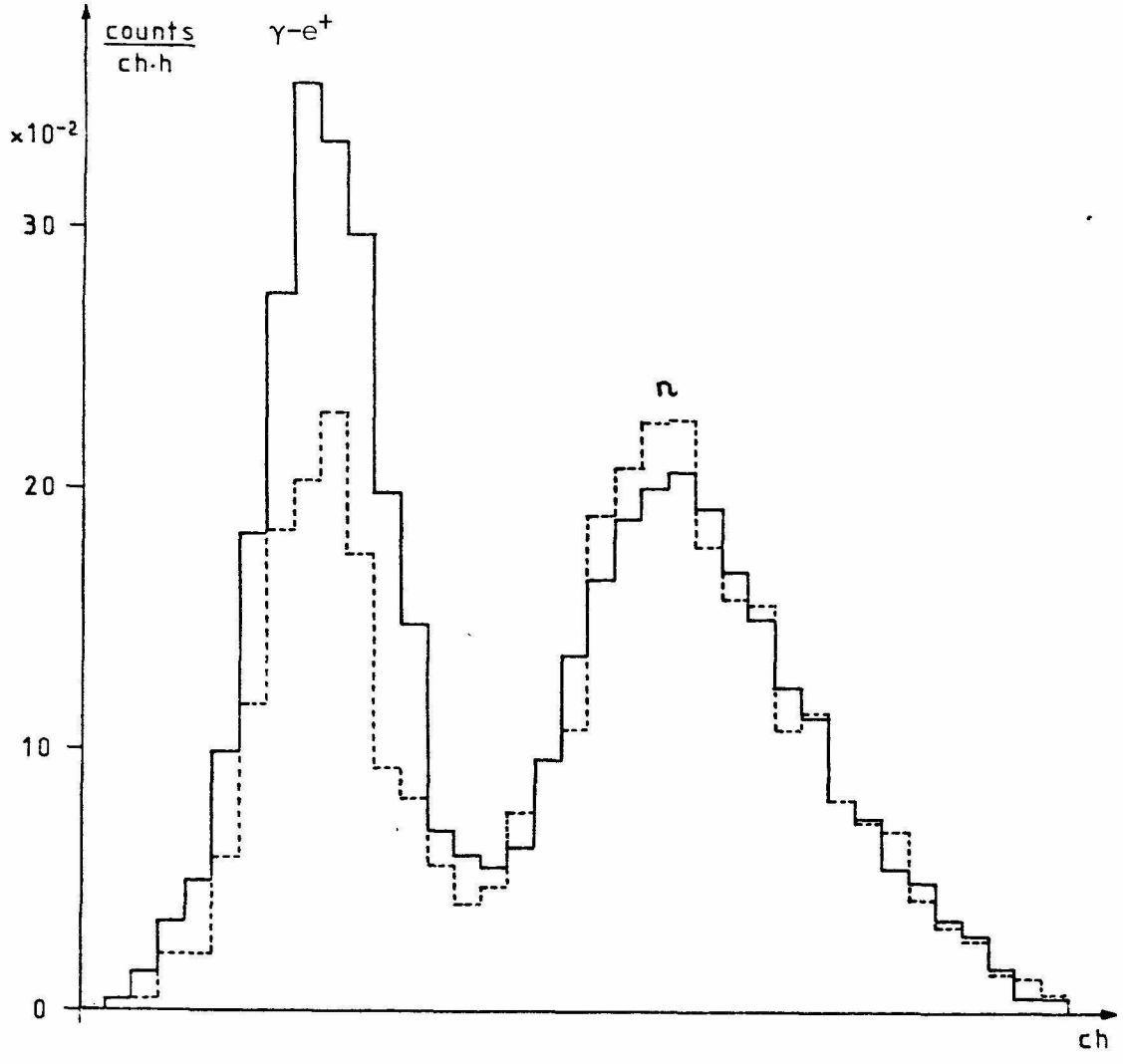

Fig. 15a: The PSD spectra of reactor-off (dotted line) and reactor-on (solid line) for 1.3 - 2.7 MeV. For reactor-on the γ-e^+ peak is enhanced due to neutrino-induced positrons. Note that the areas under the neutron peak are the same for reactor-on and reactor-off.

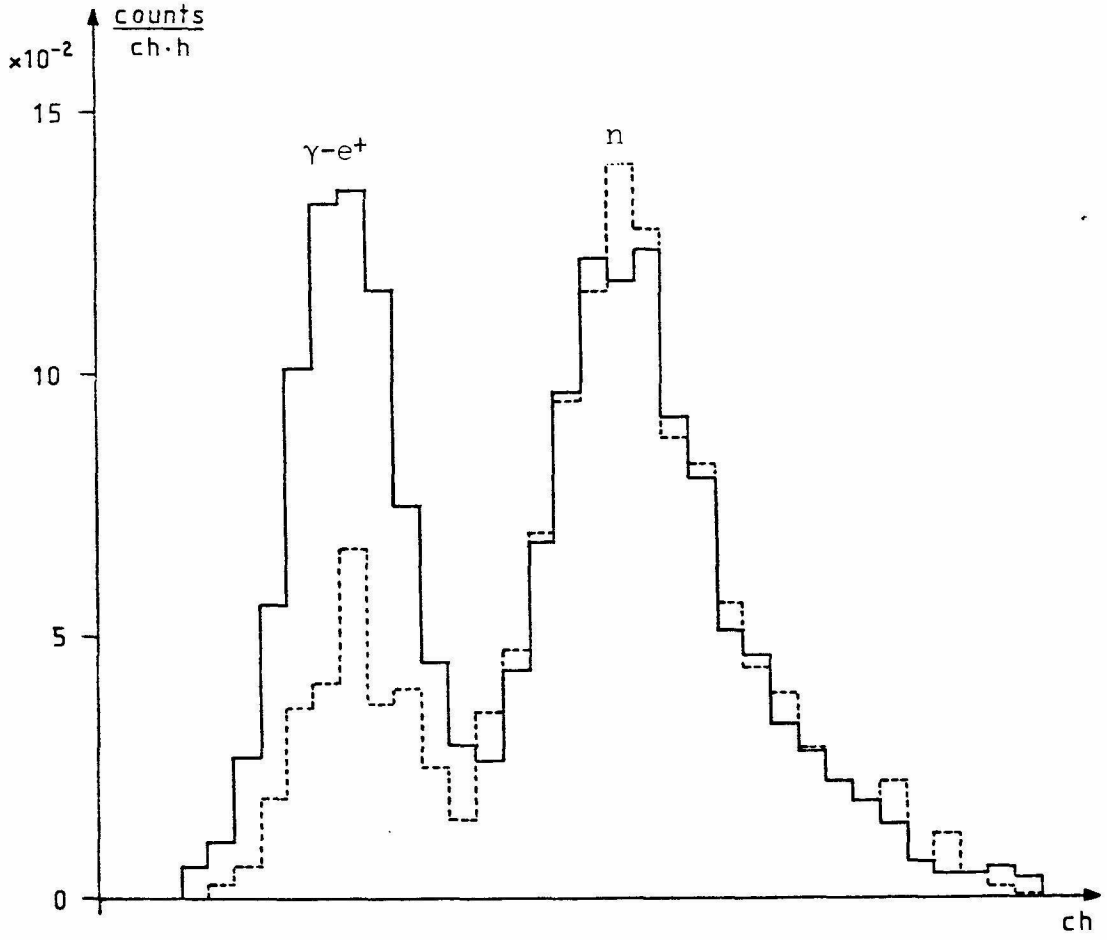

Fig. 15 b: The PSD spectra of reactor-off (dotted line) and reactor-on (solid line) for 2.7 - 4.2 MeV. For reactor-on the γ-e^+ peak is enhanced due to neutrino-induced positrons. Note that the areas under the neutron peak are the same for reactor-on and reactor-off.

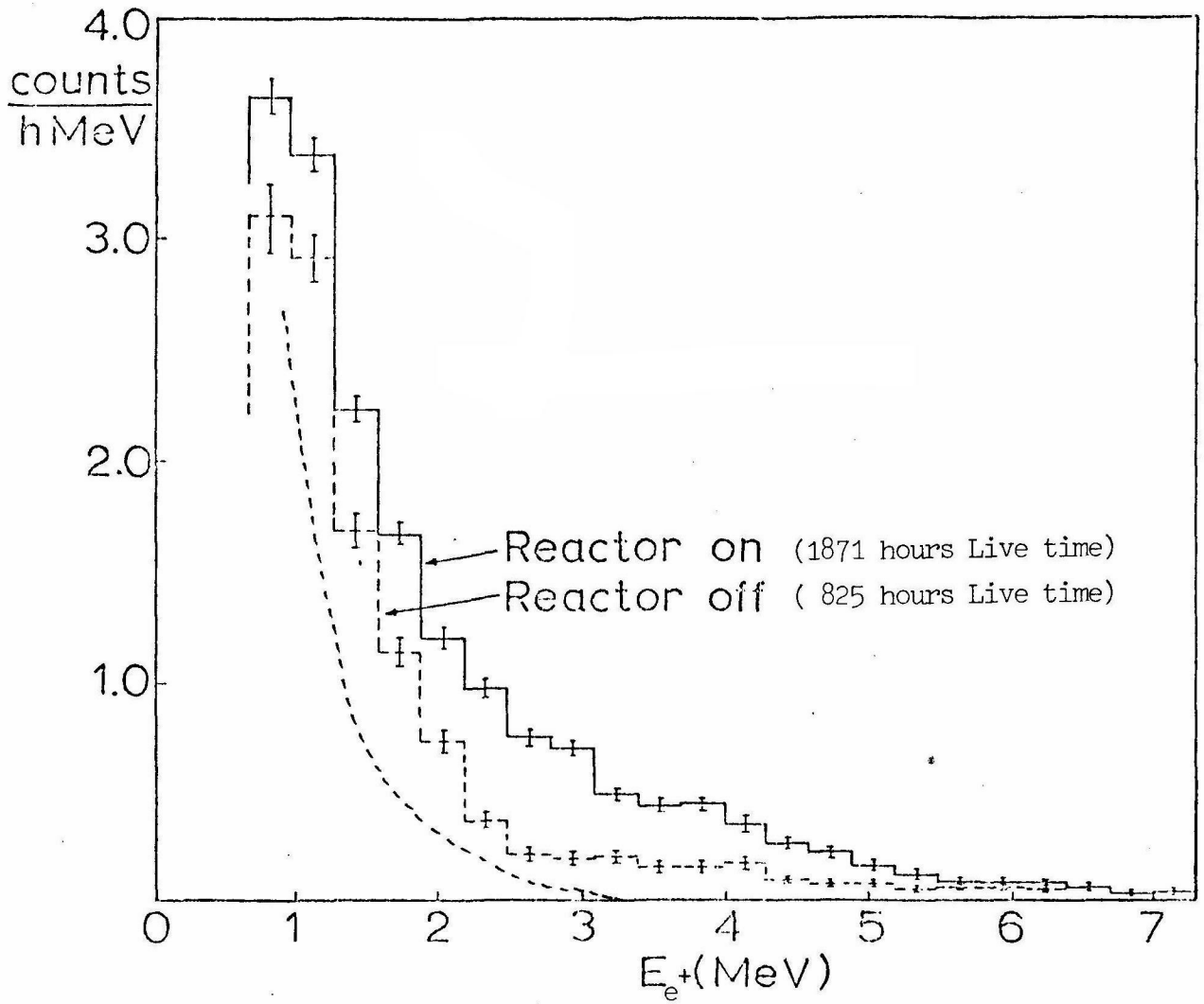

Fig. 16: The energy spectra for reactor-on and reactor-off. The accidental background is shown as a dotted line.

b) Stability Checks

The ^{3}He singles rate (within the energy window) with long veto (320 μs) anticoincidence are shown in the fourth column of the Table 3. When the reactor is on, one expects 5 ± 1 c/hr more counts in the ^{3}He counters due to neutrons from neutrino induced events in the target cells and the veto tanks. This rate was subtracted in the fourth column of the Table 3 when the reactor is on. The examination of the reactor-on and reactor-off data, shows that the stability of the ^{3}He counters is better than 1%. In total, the count rates for reactor-on and reactor-off differ by (1.1 ± 0.8)%. If this is interpreted as reactor associated single neutron events, this could increase the accidental background by (1.1 ± 0.8)%. The contribution of this to the total background is thus less than 1%, which is negligible.

The column 5 of the Table 3 shows ^{3}He singles rates in coincidence with the long veto (rejected by long veto in the analysis; condition 5). These are the neutrons related to the cosmic rays. No change is seen whether the reactor is on or off which shows that the shielding conditions are the same.

The target cell singles rates are much higher than the ^{3}He rates (Table 1 col. 3) and independent of the reactor operation. The steep energy spectrum of the singles in the target cell (Fig. 16) is used to test the stability of the detector and the electronics. The target cell events which come between 1 ms and 7 ms before the ^{3}He event are used. Except for this time window and the condition 8), all other standard cuts are made. The spectrum obtained here has good statistical accuracy.

Reactor Cycle	Reactor Status	Data taking (Real time in h)	^{3}He count rates		Target cell count rates	
			antied with V_L	coinc. with V_L	1.0-1.3 MeV	1.3-2.7 MeV
7th, 1979	OFF	291.52	245.96±0.92	439.31±1.23	42.04±0.40	34.85±0.36
1st, 1980	ON	639.07	246.75±0.63	434.85±0.82	42.02±0.28	34.66±0.25
"	OFF	202.63	244.22±1.10	433.17±1.46	38.51±0.46	32.85±0.42
2nd, 1980	ON	584.73	250.51±0.66	437.80±0.87	39.07±0.27	33.23±0.26
"	OFF	221.37	248.69±1.06	429.59±1.39	38.79±0.44	32.98±0.40
3rd, 1980	ON	471.75	250.97±0.74	438.76±0.96	37.52±0.31	32.32±0.28
"	OFF	254.75	245.40±0.98	432.60±1.30	38.33±0.41	33.95±0.38
4th, 1980	ON	643.37	247.89±0.67	427.83±0.82	40.06±0.29	35.53±0.27
TOTAL	ON	2338.91	248.70±0.33	434.45±0.43	39.84±0.14	34.04±0.13
TOTAL	OFF	970.27	246.07±0.50	433.82±0.67	39.59±0.21	33.77±0.19
TOTAL	ON-OFF		2.63±0.60±1.96*	0.63±0.80	0.25±0.25	0.27±0.23

Table 3: The rates of the ^{3}He counters and the target cells for stability checks. The errors shown are statistical errors only except for the error with an asterisk (*) which is the instrumental stability error. The symbol V_L means 320 μs long veto signal as explained in the text.

It is sensitive to the gain shift of the target cells, to the rates of the ^{3}He counters, the vetos and the umbrellas, and to the stability of the electronics.

The 6th and the 7th column of the Table 3 show these target cell event rates for two different energy bins. Since these rates are proportional to the ^{3}He count rates, they were corrected for the neutrino induced neutrons when the reactor is on (2% correction).

It is shown that the accidental background is stable to ± 1%. As a whole, the reactor-on and reactor-off spectra differ by less than 1%.

It is concluded that the detectors are stable to within 1%. Given the good signal to background ratio, this does not lead to any significant uncertainty on the positron spectrum.

3.7. BACKGROUNDS

The backgrounds for this experiment are summarized in this section.

a) Reactor Associated Background

i) Accidental Component

From the discussions of the last section, there is no significant reactor associated accidental background (less than 1% of the total background).

ii) Correlated Component

The last column of the Table 2 shows that the fast neutron events (events which are discriminated by the PSD) are the same for reactor-on and reactor-off. This can also be seen from the Fig. 15 (the neutron

peaks). This proves that there are no fast neutron events associated with the reactor. From the result of the differential shielding test (under shielding of Sec. 3.3), it is concluded that there are no slow neutrons which can make a correlated event.

Thus it is shown that there is no significant reactor associated background.

b) Reactor Independent Background

The reactor independent background is the only significant background in this experiment. It was measured during the reactor off periods. The result of the measurement is shown in Fig. 16, with the accidental component given by a dotted line. One important contribution to the accidentals comes from the ^{40}K contamination (1.46 MeV gamma rays) from the glass of the photomultiplier tubes. The backgrounds above 3 MeV are all correlated ones and are due to the cosmic rays.

CHAPTER 4

RESULTS AND DISCUSSION

In this chapter, the experimental positron spectrum is obtained and analyzed in terms of the parameters of neutrino oscillations.

4.1. EXPERIMENTAL POSITRON SPECTRUM

Since it has been shown that there is no reactor associated background, the experimental positron energy spectrum is obtained by subtracting the reactor-off spectrum from the reactor-on spectrum. The resulting positron spectrum is shown in Fig. 17 with statistical errors only. The signal to background ratio is 1:1 at 2 MeV and better above that energy. In total, 2919 ± 131 neutrino induced events have been detected with a counting rate of 1.56 ± .07 hr^{-1} (live time) for $E_{e^+} > 1$ MeV.

The theoretical positron spectrum for no oscillation is also plotted in Fig. 17.

4.2. SYSTEMATIC ERRORS

In this section, systematic errors affecting the positron spectrum are summarized. All are relative errors.

1) The uncertainty in the normalization of the intensity of the anti-neutrino energy spectrum (10%).

2) The uncertainty in the detection efficiency (8%), mainly due to the uncertainty in the neutron detection efficiency.

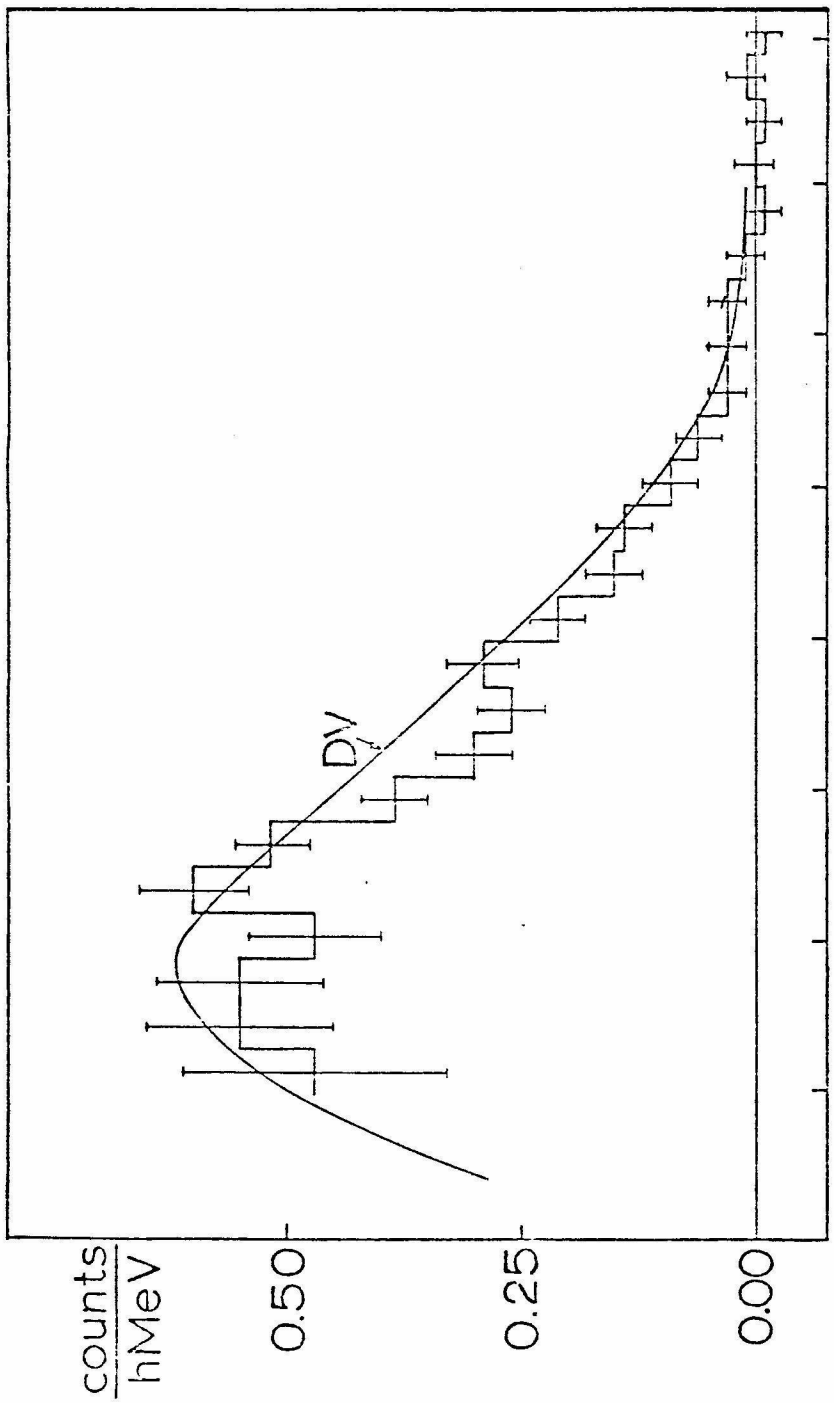

Fig. 17: The positron energy spectrum. The solid curve represents the expected positron spectrum based on the DV antineutrino spectrum.

3) As a consequence of the 2% uncertainty in the absolute energy calibration, distortions of the spectrum are possible. They are less than 4% at 4.5 MeV and 1% at 3 MeV in the amplitude.

4) The uncertainty in the inverse beta decay cross section (1.2%) (see Appendix A).

5) The uncertainty in the energy per fission (1%).

6) The stability of the reactor power (less than 1%).

7) All other uncertainties (less than 2%).

There is a resulting 13% total systematic error which is essentially energy independent.

4.3. RESULTS AND DISCUSSIONS

The ratio of the integral positron yield of the experiment to the theory is

$$\int Y_{exp}(E_{e^+})dE_{e^+} / \int Y_{th}(E_{e^+})dE_{e^+} = 0.89 \pm 0.04 \text{ (statistical)} \pm 0.13 \text{ (systematic and theoretical).}$$

The ratio of the experimental positron spectrum to the theoretical one is plotted in Fig. 18. This is to be compared with the neutrino oscillation function derived in chapter 2 for two-neutrino mixing, corrected for the instrumental response:

$$R(E_{e^+}) = \frac{\int Y(E_{e^+})P(E_\nu,d,\Delta^2,\theta)g(E_{e^+},E')h(d')dE'dd'}{\int Y(E_{e^+})g(E_{e^+},E')h(d')dE'dd'}$$

where $Y(E_{e^+})$ is the expected positron spectrum with no oscillations, $P(E_\nu,d,\Delta^2,\theta)$ is the oscillation function derived in Chapter 2, $g(E_{e^+},E')$ is the detector response function which is a Gaussian

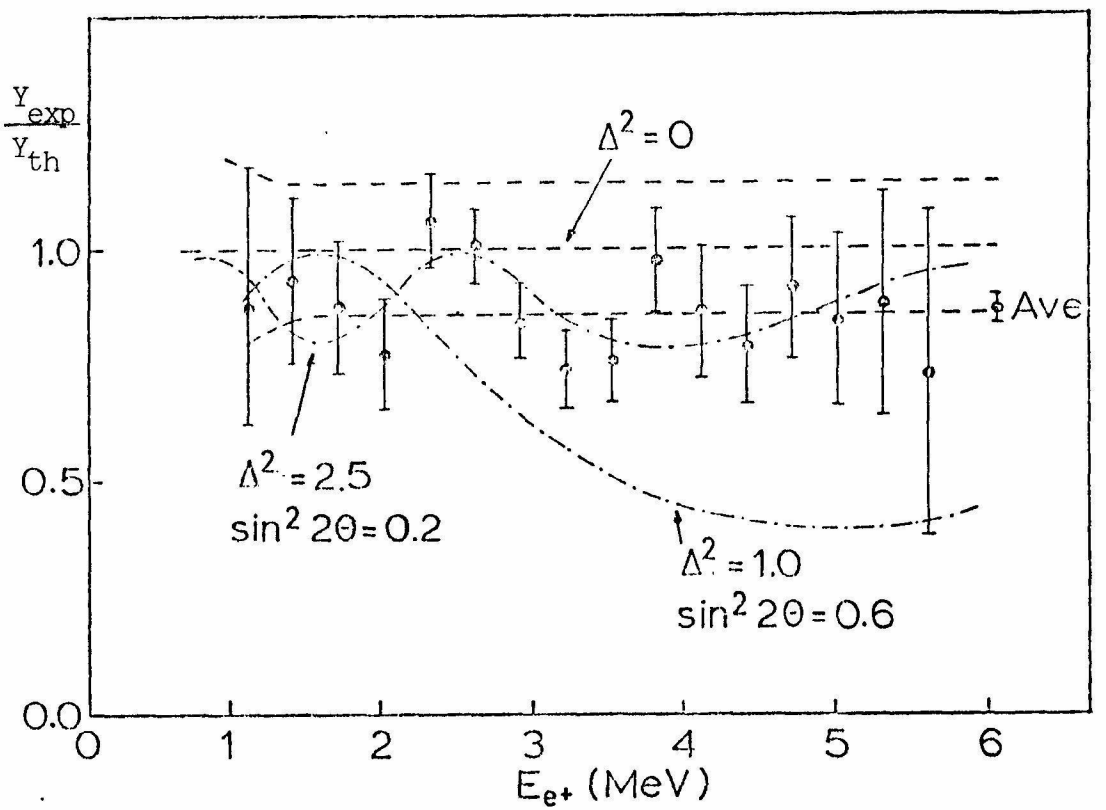

Fig. 18: The ratio of the experimental to the theoretical positron yield. The errors shown with data points are statistical errors only. The systematic errors are given by the dotted bands as explained in the text. The two dot-dashed curves illustrate the curves for different values of Δ^2 and $\sin^2 2\theta$ as explained in the text.

function in the first approximation given by,

$$\exp[-\frac{1}{2}\frac{(E_{e^+} - E')^2}{\sigma}]$$

with $\sigma = (0.9) \times (2\ell n2)^{\frac{-1}{2}} \times \sqrt{E_{e^+}}$ (Mev).

h(d') is the weighting factor for the distance d'.

A chi-square test of $R(E_{e^+})$ as a function of Δ^2 and $\sin^2 2\theta$ was made to the data of the Fig. 18. Since there is a 13 % uncertainty on the normalization of the spectrum, the amplitude of the spectrum was allowed to vary within this uncertainty (between the dotted bands in Fig. 18), and the lowest value of χ^2 was taken. The 68% and 90% confidence level curves of the Δ^2 vs. $\sin^2 2\theta$ are plotted in Fig. 19. The regions to the left of the curves are the allowed ones.

The experimental data are consistent with no oscillations. At maximum mixing, a limit of

$$\underline{\Delta^2 = 0.2(eV)^2 \text{ (90\% confidence level)}}$$

is achieved. If the mixing angle is small, various solutions are possible. Two examples of the oscillation curves are shown in Fig. 18. One is for $\sin^2 2\theta = 0.2$, $\Delta^2 = 2.5(eV)^2$ which obviously is an allowed solution. The other is for $\sin^2 2\theta = 0.6$, $\Delta^2 = 1.0\ (eV)^2$, the value favored by the data of Reines et al. described as follows.

Recently, Reines et al.[16], reported evidence for neutrino instability. The group measured the cross section for the antineutrino

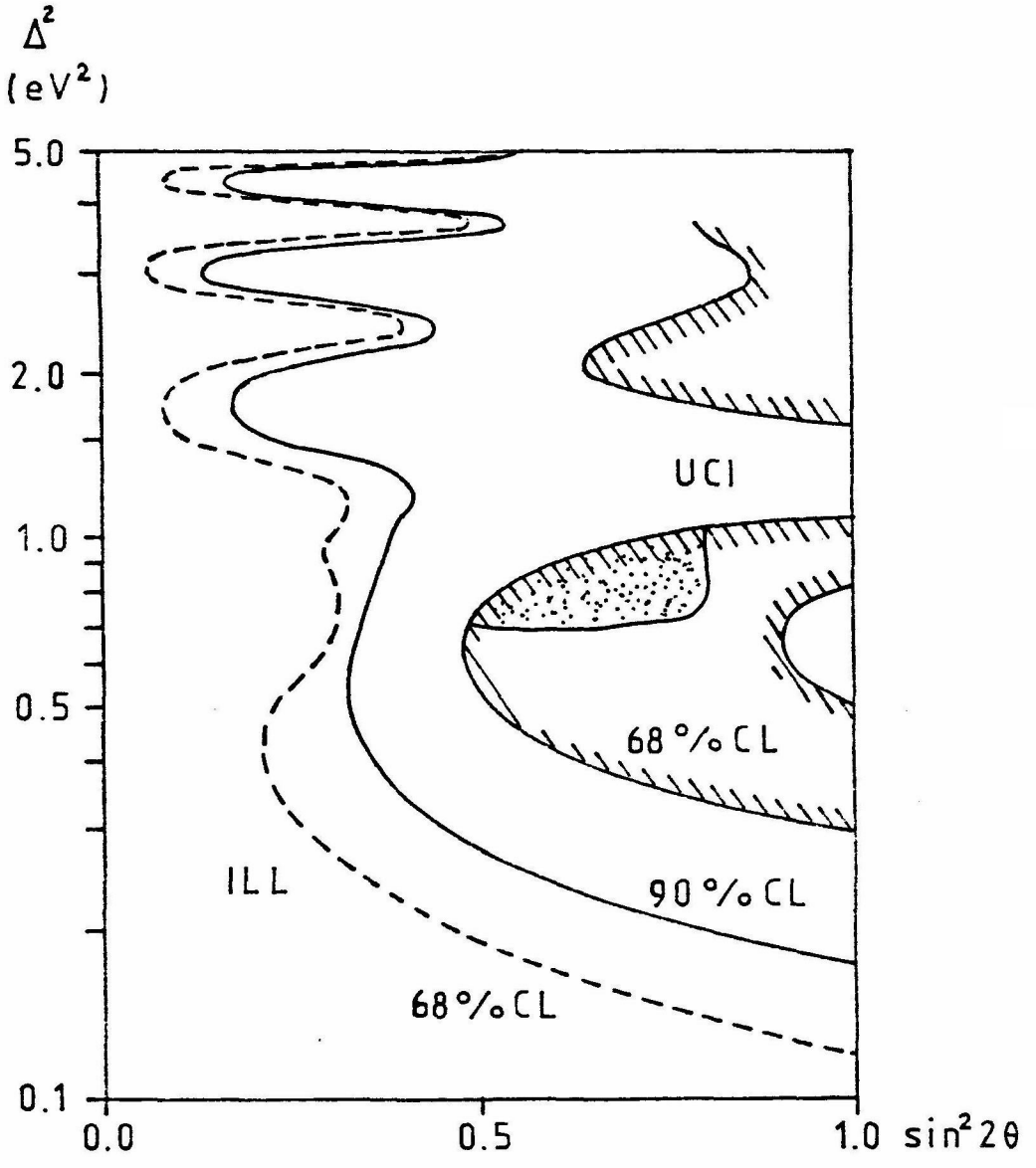

Fig. 19: The limits on the neutrino-oscillation parameters Δ^2 vs.$\sin^2 2\theta$ given by this experiment at ILL. The regions to the right of the curve can be excluded. The allowed regions claimed by Reines et al., from $\bar{\nu}_e$d experiment are shown as a shaded area. A restricted region as explained in the text is sketched as a dotted area. Note that Reines et al., used the AG spectrum instead of the DV spectrum to get this plot.

induced disintegration of the deuteron both via a charged current (CC) and a neutral current (NC) reaction:

$$\bar{\nu}_e + d \begin{cases} \rightarrow n + n + e^+ & CC \\ \rightarrow n + p + e^+ & NC \end{cases}$$

The "ratio of ratios"

$$RR = \frac{(Y_{CC}/Y_{NC})exp}{(Y_{CC}/Y_{NC})_{th}}$$

was measured where Y_{CC} is the yield of double neutrons due to CC reaction and Y_{NC} is the yield of single neutrons due to NC reaction.

The following result was found:

$$RR = 0.40 \pm 0.22.$$

Since this is a relative measurement, it is expected to be less sensitive to the detector efficiency and the antineutrino spectrum.

For flavor oscillations of neutrinos, the NC reaction will occur no matter what kind of neutrino interacts with the deuteron while the CC reaction can only be induced by $\bar{\nu}_e$ (the threshold for other neutrinos is too high). Interpreting the result for RR in terms of two neutrino flavor oscillations, the authors determined a set of values for Δ^2 and $\sin^2 2\theta$ as shown in Fig. 19. By combining all their previous experiments and using the AG spectrum[22], they found a restricted region which is also sketched in Fig. 19.

In their data, they give the ratio of the measured $\bar{\nu}_e$ spectrum

from $(\bar{\nu}_e + d)_{cc}$ reaction to their own measured $\bar{\nu}_e$ from $(\bar{\nu}_e + p)$ reaction was reported to be 0.56 ± 0.27. Since this ratio should be 1 (because it is the same mechanism except that the proton is bound in the deuteron for the CC reaction), there appears to be an inconsistency[32].

Further independent checks of the deuteron experiments thus are necessary before definite conclusions can be drawn.

Additional suggested evidence for neutrino oscillations from the CERN beam dump and from Serpukov experiments were submitted to the Neutrino-80 Conference[33] at Erice, Italy. As these works are still subject to criticism and not free of inconsistencies, they will not be discussed in this thesis.

In conclusion, the present experiment furnishes stringent limits on the neutrino-oscillation parameters, Δ^2 and $\sin^2 2\theta$. The results are consistent with no oscillation, or with oscillations with a small mixing angle.

CHAPTER 5

FUTURE PROSPECTS

To improve the sensitivity for the oscillation parameters, further work is necessary at fission reactors. Clearly one can be independent of the uncertainty in the calculated antineutrino spectrum by making the detector movable and by measuring the spectrum at two or more different positions.

To move the present detector to another positon at ILL which will be further away from the reactor core, it is imperative to reduce the background. This can be achieved by making the target cells and the ^3He counters position sensitive and thus localizing the neutrino events. It is anticipated that this will reduce the accidental as well as the correlated background. Even then, one is limited by lower counting rate.

On the other hand, a power reactor provides a much stronger antineutrino source. In addition, by increasing the source-detector distance, a better sensitivity for Δ^2 can be obtained. By measuring at 40 m and 70 m positions from the 2700 MW Gösgen reactor, it appears possible to achieve a sensitivity for Δ^2 as low as 0.03 eV^2 assuming maximum mixing ($\theta = \frac{\pi}{4}$). Such a project is in fact in progress by a collaboration of Caltech, SIN (Swiss Institute for Nuclear Research), and T.U. München.

APPENDIX A: Derivation of the $\bar{\nu}_e + p \rightarrow e^+ + n$ Cross Section

The cross section of the process

$$\bar{\nu}_e + p \rightarrow e^+ + n$$

is derived for low energy (few MeV) antineutrinos using the matrix element of the free neutron decay. The energy of the product neutron is only about 10 keV which is negligible. Therefore the positron energy (total energy; not kinetic energy) is related to the antineutrino energy by,

$$E_{e^+} = E_{\bar{\nu}} - E_o$$

where $E_o = (m_n - m_p)c^2 = 1.29$ MeV.

From Fermi's golden rule, we have;

$$d\Gamma = \text{transition probability per second}$$
$$= \left(\frac{2\pi}{\hbar}\right)|H_{fi}|^2 \, \delta(E_{\bar{\nu}} - E_{e^+} - E_o) \, \frac{d^3 P_{e^+}}{(2\pi\hbar)^3}$$

where $H_{fi} = \langle e^+ n | H | \bar{\nu}_e p \rangle$

$$= G_F M.$$

In the low energy approximation, the matrix element M is independent of the positron momentum.

$d\Gamma$ is related to the cross section $d\sigma$ by,

$$d\Gamma = d\sigma\left(\frac{E_{\bar{\nu}}}{P_{\bar{\nu}}}\right) .$$

Therefore the cross section $d\sigma$ is given by,

$$d\sigma = \left(\frac{2\pi}{\hbar}\right)|H_{fi}|^2 \, \delta(E_{\bar{\nu}} - E_{e^+} - E_o) \, \frac{d^3 P_{e^+}}{(2\pi\hbar)^3}.$$

Integrating over the phase space, we have

$$\sigma(E_{\bar{\nu}}) = \frac{G_F^2 |M|^2}{\pi^2 \hbar^4 c^4} \, (E_{\bar{\nu}} - E_o) \sqrt{(E_{\bar{\nu}} - E_o)^2 - (m_e c^2)^2}.$$

Now $G_F^2 |M|^2$ is obtained from the lifetime of the free neutron;

$$f\tau_n = \frac{2\pi^3 h^7}{m_e^5 c^4 G_F^2 |M|^2}$$

where $f = 1.71573 \pm 0.00030$ [34] is the phase space factor and $\tau_n = 926 \pm 11$ sec [35] is the mean lifetime of the neutron.

Thus the cross section as a function of antineutrino energy is given by,

$$\sigma(E_{\bar{\nu}}) = \left(\frac{2\pi^2}{c}\right)\left(\frac{h}{m_e c}\right)^3 \cdot \frac{1}{(m_e c^2)^2}(E_{\bar{\nu}} - E_o) \sqrt{(E_{\bar{\nu}} - E_o)^2 - (m_e c^2)^2}.$$

$$= (9.13 \pm 0.11) \times (E_{\bar{\nu}} - 1.29)\sqrt{(E_{\bar{\nu}} - 1.29)^2 - (0.511)^2} \times 10^{-44} \text{ cm}^2$$

where $E_{\bar{\nu}}$ is in units of MeV.

APPENDIX B: Calculation of the Neutron Detection Efficiency

To calculate the overall neutron detection efficiency, the target cells are divided into 4 groups (A to D) according to their positions as shown in Fig. B.1. The efficiency of the target cells in each group is identical and depends on whether the neutrons can escape out of the detector along the length, height or width of the cells. The efficiencies for each group can be written as follows;

$$\varepsilon_A = \varepsilon_o \eta_L$$
$$\varepsilon_B = \varepsilon_o \eta_L \eta_H$$
$$\varepsilon_C = \varepsilon_o \eta_L \eta_W$$
$$\varepsilon_D = \varepsilon_o \eta_L \eta_H \eta_W$$

where ε_o is the efficiency for the center of the target cell, and η_L, η_H, η_W are the correction factors for the length, height and the width, respectively, of the target cell.

These values are obtained from the Fig. 10 and Fig. 11 and given by,

$$\varepsilon_o = 0.40 \pm .014$$
$$\eta_L = 0.87 \pm .02$$
$$\eta_H = 0.75 \pm .03$$
$$\eta_W = 0.50 \pm .04.$$

Then the overall efficiency is given by

$$\bar{\varepsilon} = \frac{1}{30}(12\ \varepsilon_A + 6\ \varepsilon_B + 8\ \varepsilon_C + 4\ \varepsilon_D)$$

$$= (25.6 \pm 2.1)\%.$$

Since only the ^{3}He counter ## 3 and ## 4 (Fig. B.1) were used in the efficiency measurement, and since the ^{3}He counter ## 1 and # 2 have different efficiencies,an additional correction has to be made. It was determined by measuring the integral count rate with a neutron source in two symmetric positions.

Finally the efficiency is obtained as,

$$\varepsilon(t=\infty) = (24.9 \pm 2.1)\%$$

or the efficiency within 200 μs coincidence window is then given by,

$$\underline{\varepsilon(200\ \mu s) = (20.2 \pm 1.7)\ \%}.$$

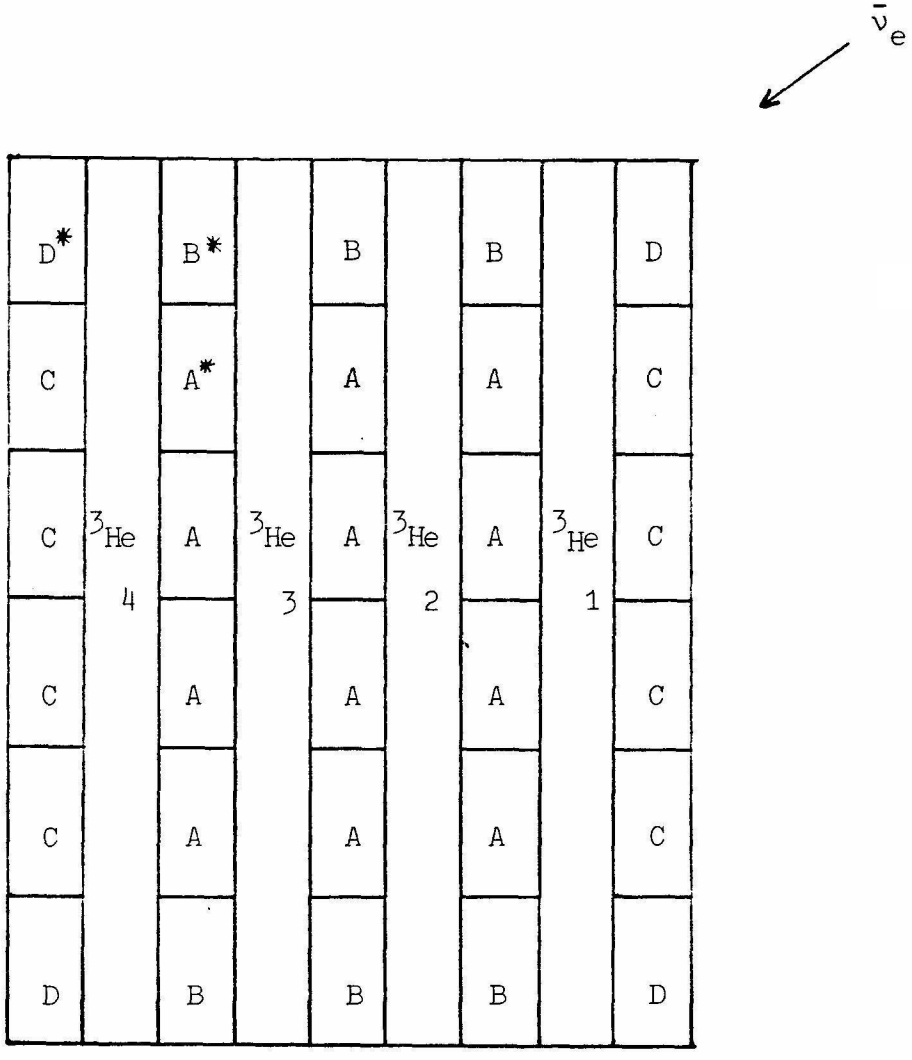

Fig. B.1. Target cells in different efficiency groups (A-D). The investigated target cell positions are shown with an asterisk (*).

APPENDIX C: The Drawings of the Veto Tanks

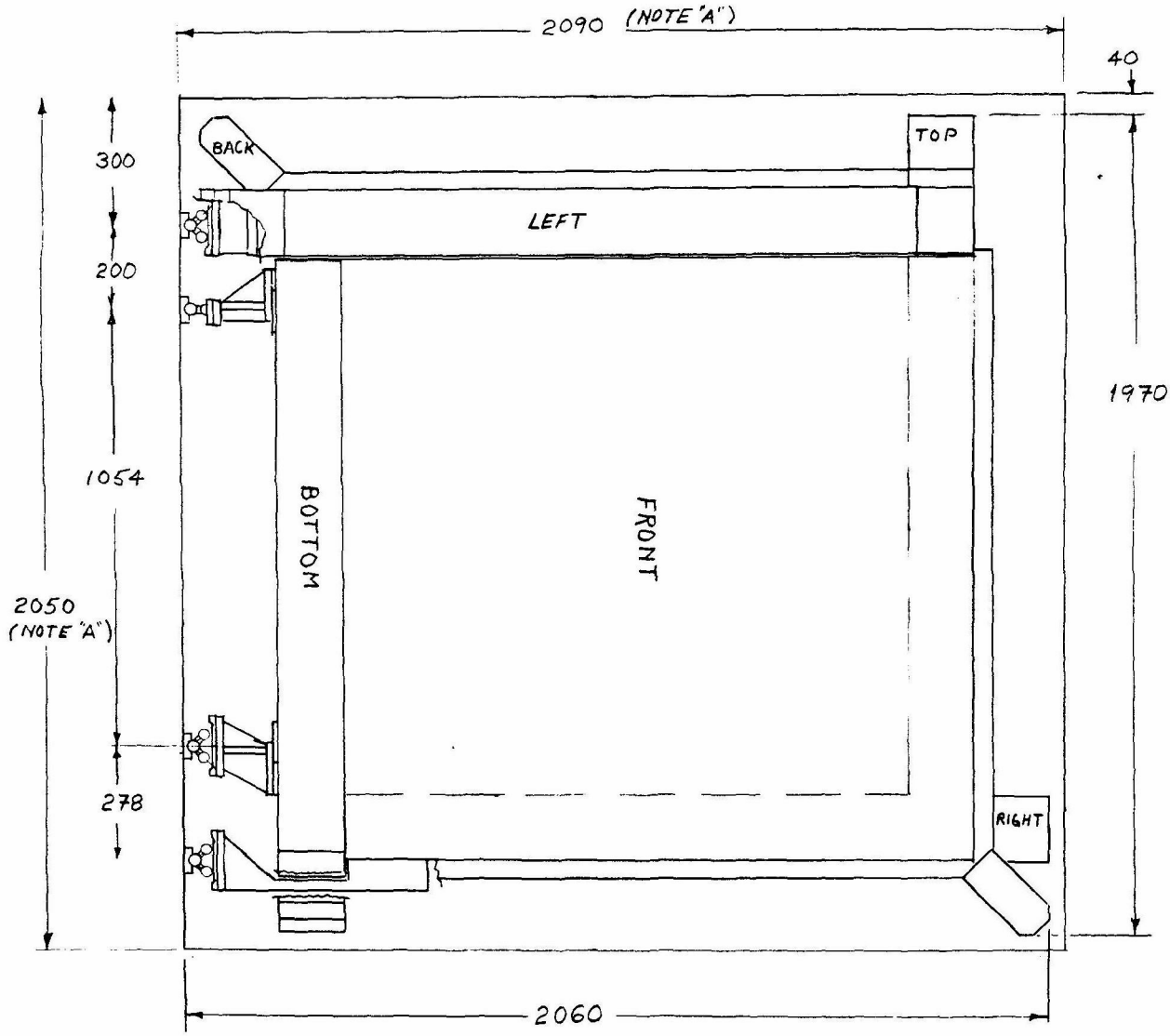

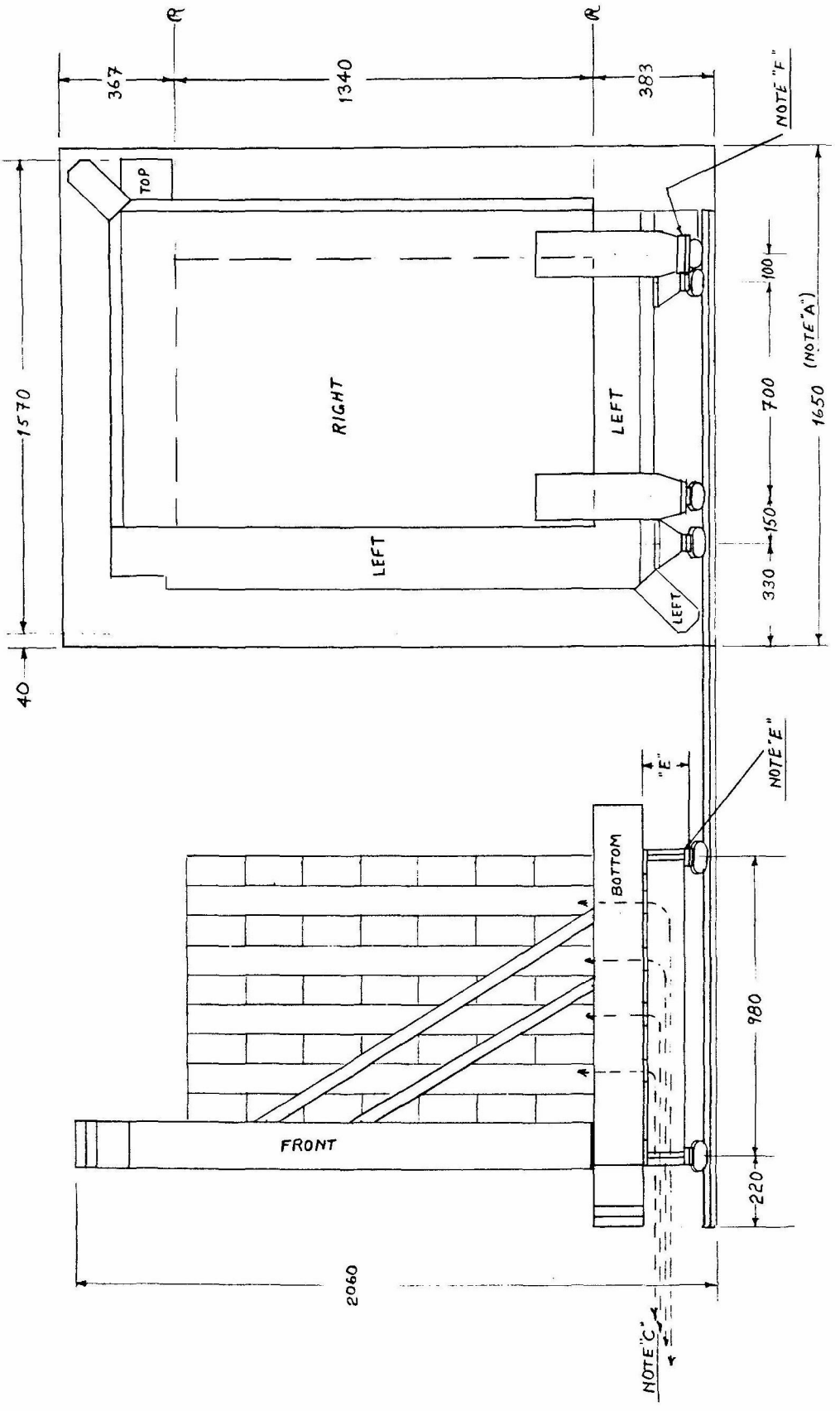
367
1340
383
NOTE "F"
TOP
RIGHT
LEFT
LEFT
LEFT
1570
40
100
700
150
330
1650
(NOTE "A")
NOTE "E"
"E"
BOTTOM
FRONT
980
220
2060
NOTE "C"

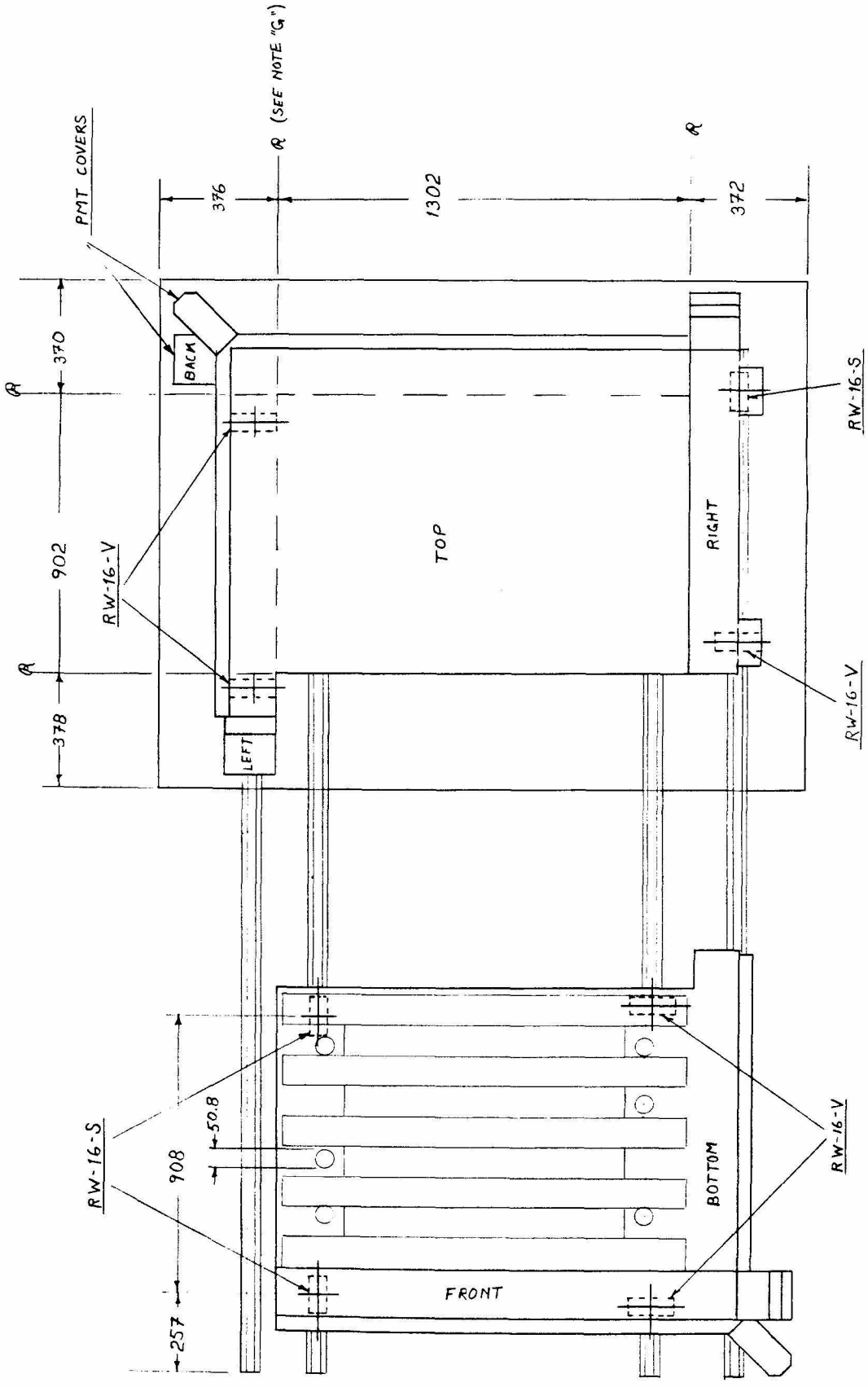
PMT COVERS
℄ (SEE NOTE "G")
376
1302
372
℄
370
℄
902
℄
378
BACK
LEFT
TOP
RIGHT
BOTTOM
FRONT
RW-16-V
RW-16-S
RW-16-V
RW-16-S
RW-16-V
50.8
908
257

REFERENCES

1) M. Nakagawa et al., Prog. Theo.Phys. 30, 727 (1963)
Y. Katayama et al., Prog. Theo.Phys. 28, 675 (1962)
Z. Maki et al., Prog. Theo. Phys. 28, 870 (1962)

2) G. Danby et al., Phys. Rev. Lett. 9, 36 (1962)

3) V. Gribov and B. Pontecorvo, Phys. Lett. 28B, 493 (1969)

4) A review about solar neutrinos can be found in
J.N. Bahcall, Rev. Mod. Phys. 50, 881 (1978) and references therein

5) H. Fritzsch,
in: Fundamental Physics with Neutrons and Neutrinos p. 117
edited by T. von Egidy, Inst. Physics, Bristol and London (1978)

6) S.M. Bilenky and B. Pontecorvo, Phys. Report 41, 225 (1978)
Neutrino oscillations were discussed by various authors:
L. Wolfenstein, Phys. Rev. D20, 2634 (1979)
J.N. Bahcall and H. Primakoff, Phys. Rev. D18, 3463 (1978)
H. Fritzsch and P. Minkowski, Phys. Lett. 62B, 72 (1976)
S.M. Bilenky and B. Pontecorvo, Phys. Lett. 61B, 248 (1976)
S. Eliezer and A.R. Swift, Nucl. Phys. B105, 45 (1976)
S. Eliezer and D.A. Ross, Phys. Rev. D10, 3088 (1974)
J.N. Bahcall and S.C. Frautschi, Phys. Lett. 29B, 623 (1969)

7) Neutrino masses in the Grand Unification Theories are discussed in,

M. Magg and Ch. Wetterich, Phys. Lett. 94B, 61 (1980)

A. Zee, Phys. Lett. 93B, 389 (1980)

E. Witten, Phys. Lett. 91B, 81 (1980)

R. Barberi et al., Phys. Lett. 90B, 91 (1980), ibid p. 249 (1980)

R.N. Mohapatra and G. Senjanovic, Phys. Rev. Lett. 44, 912 (1980)

R.N. Mohapatra and R.E. Marshak, Phys. Rev. Lett. 44, 1316 (1980)

8) S. Glashow, Nucl. Phys. 22, 22 (1961)

A. Salam and J. Ward, Phys. Lett. 13, 168 (1964)

S. Weinberg, Phys. Rev. Lett. 19, 1264 (1967)

9) E.F. Tretiakov et al., preprint ITEP No. 15, Moscow 1976

10) M. Daum et al., Phys. Lett. 74B, 126 (1978)

11) W. Bacino et al., Phys. Rev. Lett. 42, 749 (1979)

12) V.A. Lyubimov et al., Phys. Lett. 94B, 266 (1980)

13) R. Cowsik and J. McClelland, Phys. Rev. Lett. 29, 669 (1972)

B.W. Lee and S. Weinberg, Phys. Rev. Lett. 39, 165 (1977)

P. Hut and K.A. Olive, Phys. Lett. 87B, 144 (1979)

14) D. Schramm and G. Steigman, Phys. Lett. 87B, 141 (1979)

15) S. Weinberg, Address at Neutrino-78 (Purdue Univ., 1978)

16) F. Reines et al., preprint UCI-10P19-144 (1980)

17) A more general discussion can be found in
A. DeRujula et al., preprint TH-2788-CERN (1979)

18) An estimation is made in Ref. 6 for a possible $\nu_1 \rightarrow \nu_2 + \gamma$ decay and results that the life time of ν_1 is greater than the age of the universe.

19) Series of reactor $\bar{\nu}_e + p \rightarrow e^+ + n$ experiments were done by,
F. Reines and C.L. Cowan Jr., Phys. Rev. 92, 830 (1953)
F. Reines and C.L. Cowan Jr., Phys. Rev. 113, 273 (1959)
F. Reines, C.L. Cowan Jr. et al., Phys. Rev. 117, 159 (1960)
F.A. Nezrick and F. Reines, Phys. Rev. 142, 852 (1966)

20) Reactor Handbook vol. III. p. 4. Second Edition, Interscience publisher (1962)

21) B.R. Davis, P. Vogel, F.M. Mann and R.E. Schenter, Phys. Rev. C19, 2259 (1979)

22) F.T. Avignone III and Z.D. Greenwood, preprint Univ. South Carolina (1980)

23) K. Schreckenbach et al., to be published.

24) J.K. Dickens, preprint, Oak Ridge Natl. Laboratory,(September, 1980)

25) A review on PSD as well as a general discussion on organic scintillators can be found in
F.D. Brooks, Nucl. Inst. Meth. 162, 477 (1979)

26) Charles Hurlbut, Nuclear Enterprises, Inc., San Carlos Calif. 94070 USA

27) G. Keil, Nucl. Inst. Meth. 87, 111 (1970)

28) B. Barish et al., preprint Caltech Calt-68-623 (1968)

29) G.Champion, thesis at ISN (Institut des Sciences Nucléaire de Grenoble) (1979)

30) The source was made by Amersham,
The Radiochemical Centre Ltd.,Withe Lion road
Amersham, Buckinghamshire, HP7 9LL, England

31) Tables of Isotopes, p. 602,Seventh Edition,John, Wiley and Sons Inc (1978)

32) R.P. Feynman and P. Vogel, private communication.

33) F. Boehm et al., contribution to Neutrino-80 conference at Erice, Italy (1980)

34) D.H. Wilkinson, Symmetries and Nuclei, in: Nuclear physics with heavy ions and mesons Vol. I., eds. R. Balian et al. (North-Holland, Amsterdam, 1978)

35) C.J. Christensen et al., Phys. Rev. D5, 1628 (1972)
J. Byrne et al., Phys. Lett. 92B, 274 (1980)

POST APPENDIX: The Journalism

Nature Vol 286 21 August 1980

Neutrino weight watching

from A. De Rújula and S.L. Glashow

The Laue-Langevin experiment started running last November and will end this summer. The group, consisting of Felix Boehm, J. F. Cavaignac, D. H. Koang and B. Vignon (Institut des Sciences Nucleaires, Grenoble) and Franz von Feilitzsch and Rudolf Mossbauer (Technical University, Munich), also measured the neutrino-induced reaction on the proton. Their detector, placed 8.7 meters from the core, was a proton-rich scintillator (375 liters) that acted simultaneously as target, positron detector and neutron moderator. He^3 wire chambers detect neutrons in coincidence with positrons. Their signal-to-noise ratio was 1.5 and the event rate 1.5/hour.

SCIENCES ET TECHNIQUES

Inventés il y a cinquante ans, les neutrinos sont au centre de plusieurs énigmes

POUR LA PREMIÈRE

Haben die Neutrinos eine Masse?

Stetige Umwandlung zwischen verschiedenen Formen / Konsequenzen für die Astrophysik

SCIENCE AND THE CITIZEN

Neutrinos Have Mass Would Change View of Universe

Neutrinos may not be what they seem.

UCI scientists' tests may alter theories

By JULIAN LOEWE
Staff Writer

If an experiment by a group of University of California at Irvine physicists is right, a lot of modern physics theory and astrophysical beliefs about the very fabric of the universe is going to have to be revamped, a possibility that is sending ripples through physics departments throughout the world.

Dr. Elaine Pasierb, along with her colleagues *Drs. Henry Sobel and* Frederick Reines, have conducted some experiments they feel show neutrinos have mass.

Galaxies, stars, planets and all the the universe was created in this Big tronomers have held that the univers still expanding, does not have enou produce enough gravity to brake t sion. The universe, then, will expand

But neutrinos with substance woul enough gravity to stop the expansion, the universe together again, perhap eventual recreation billions or trillions from now.

There are other areas that would be as well, mysteries that would be solved.

Current theory holds the sun should p enormous numbers of neutrinos, but me

Caltech physicist: UCI group wrong on neutrinos

By JULIAN LOEWE
Staff Writer

It could shape up as a classic scientific donnybrook.

The fuel for the fight seems to come from a remarkably innocuous source: the neutrino, a particle in sub-atomic physics that has no mass, at least according to the knowledge available today.

Now, a group of physicists from the University of California at Irvine claim to have scientific proof that neutrinos do indeed have mass. And that claim, which, if true, would cause a lot of modern atomic physics to be redone, is starting to come under fire.

Physicists were loath at first to knock the results, although they did question the UCI group's work not as bad physics but because the results were released to the press before scientific documentation was made available to other physicists.

Now, however, a Caltech physicist, Felix Boehm, has stated flatly that he thinks the UCI group was wrong. Boehm didn't totally dismiss the possibility neutrinos may have mass. In fact, he is working on experiments at Granoble, France, along with other Caltech researchers and French and German co-workers to further the search.

But, Boehm told a crowded Caltech auditorium audience, the UCI group's own figures themselves show that neutrinos do not oscillate.

Oscillations are the key to the argument.

The UCI team, headed by Frederick Reines, said that neutrinos oscillated from one type of neutrino to another. If these oscillations take place, there must be something there to oscillate. That something would mean neutrinos have mass.

Boehm, who has now read preliminary reports by the Reines group, said that not only does their data actually show there are no oscillations (and hence no mass) but also, he added, the UCI data is inconsistent with the UCI report's conclusions and also with other data in the report.

Were neutrinos to have mass, a lot of mysteries in physics would be explained.

For instance, measurements on earth detect only about half the neutrinos being emitted from the sun that physics theory says there should be. If neutrinos had oscillated into types not now being measured, they wouldn't show up on the counters. The missing neutrinos would have been found.

If they had any mass at all, neutrinos would provide enough mass to reverse the Big Bang. The Big Bang theory holds that the universe was born in a primal explosion about 15 billion years ago.

Boehm said that he and others had worked at the French Grenoble nuclear study center found no evidence of oscillations. He said that the readings of neutrinos that were found coincided exactly with Davis-Vogel predictions of what those findings should have been. And the Davis-Vogel predictions showed what the results would be if there were no oscillations.

Even the UCI curves fit the Davis-Vogel curves, Boehm said. If neutrinos did oscillate, the curves would have been distinctly different.

Boehm pointed out that the Reines results also now stand alone.